SPATIAL DISTRIBUTIONS FROM 285 TO 2500°K ARGON BEAMS SCATTERED FROM AN UNDEFINED COPPER SURFACE AT TEMPERATURES BETWEEN 36 AND 285°K

R. L. Caldwell, M. R. Busby, and R. F. Brown

ARO, Inc.

December 1969

AEROSPACE ENVIRONMENTAL FACILITY
ARNOLD ENGINEERING DEVELOPMENT CENTER
AIR FORCE SYSTEMS COMMAND
ARNOLD AIR FORCE STATION, TENNESSEE

NOTICES

When U. S. Government drawings specifications, or other data are used for any purpose other than a definitely related Government procurement operation, the Government thereby incurs no responsibility nor any obligation whatsoever, and the fact that the Government may have formulated, furnished, or in any way supplied the said drawings, specifications, or other data, is not to be regarded by implication or otherwise, or in any manner licensing the holder or any other person or corporation, or conveying any rights or permission to manufacture, use, or sell any patented invention that may in any way be related thereto.

Qualified users may obtain copies of this report from the Defense Documentation Center.

References to named commercial products in this report are not to be considered in any sense as an endorsement of the product by the United States Air Force or the Government.

SPATIAL DISTRIBUTIONS FROM 285 TO 2500°K ARGON BEAMS SCATTERED FROM AN UNDEFINED COPPER SURFACE AT TEMPERATURES BETWEEN 36 AND 285°K

R. L. Caldwell, M. R. Busby, and R. F. Brown
ARO, Inc.

FOREWORD

The research presented in this report was sponsored by the Arnold Engineering Development Center (AEDC), Air Force Systems Command (AFSC), Arnold Air Force Station, Tennessee, under Program Element 61102F, Project 8951.

The results of research were obtained by ARO, Inc. (a subsidiary of Sverdrup & Parcel and Associates, Inc.), contract operator of AEDC, AFSC, under Contract F40600-69-C-0001. The research was conducted from September to November, 1968, under ARO Project No. SW3904. The manuscript was submitted for publication on May 29, 1969. This work was done under ARO Contract 69-29-TS/OMD with The University of Tennessee Space Institute (UTSI). Messrs. Caldwell and Busby were students at UTSI when most of this work was done. They are now full-time employees of ARO, Inc.

The authors wish to thank Dr. J. D. Haygood, ARO, Inc., for his valuable consultations concerning the interpretation of the data.

This technical report has been reviewed and is approved.

Michael G. Buja
2d Lt, USAF
Research Division
Directorate of Plans
and Technology

Harry L. Maynard
Colonel, USAF
Director of Plans
and Technology

ABSTRACT

An aerodynamic molecular beam and a phase-sensitive detection system were used to investigate the effects of the gas temperature, incidence angle, and surface temperature on the spatial distribution from 285 to 2500°K argon beams reflected from an undefined copper surface. With an incident beam temperature less than 1400°K, cosine scattering was observed during all of the tests. However, data were not obtained for incident angles, measured with respect to the surface normal, greater than 70 deg. With incident beam source temperatures greater than 1400°K, the scattering patterns were observed to be dependent on the angle of incidence and the incident beam energy. Low angles of incidence and high beam energies (i.e., greater than 0.30 ev) result in spatial distributions with strong lobular patterns. To determine the effects of the surface temperature on the spatial distribution, several experiments were run with a 0.54-ev incident beam at surface temperatures of 285, 131, 77, and 36°K. With a surface temperature of 285°K and an incidence angle of 70 deg, lobular reflection patterns were observed, and at 131°K the reflection patterns became more lobular. Then, with a surface temperature of 77°K, slightly lobular patterns were observed, and at 36°K the spatial distribution of the reflected beam was cosine. These data are the first known observations of lobular scattering patterns for low energy (i.e., 0.30- to 0.54-ev) beams scattered from contaminated surfaces at low temperatures. Also, the trends observed during these experiments are in agreement with the general predictions of Stickney but are in disagreement with the previous predictions that lobular scattering patterns are limited to clean, hot surfaces or to the scattering of particles with energies greater than 1 ev.

CONTENTS

APPENDIXES

I. ILLUSTRATIONS

Figure

NOMENCLATURE

A	Constant depending on γ in Eq. (III-1)
A. C.	Energy accommodation coefficient
D	Diameter of the sonic orifice
E_i	Energy of a molecule incident on the surface
E_r	Energy of a molecule reflected from the surface
E_s	Energy of a molecule in thermal equilibrium with the surface
F	Geometric correction factor
M	Mach number
m	Molecular mass
n	Molecular number density
P_o	Stagnation pressure
R	Gas constant
T_g	Temperature of the gas
T_o	Stagnation temperature
T_s	Temperature of the surface
$\vec{U}_i$	Incident velocity vector of the gas atom
$\vec{U}_r$	Reflected velocity vector of the gas atom
$\vec{V}_i$	Velocity vector of the surface atom
W_a	Width of the beam spot viewed by the detector at $\theta_i \neq 0$
W_c	Width of the chopper opening
W_D	Width of the detector entrance
W_n	Distance defined in Fig. IV-1
W_o	Width of the beam spot at normal incidence
x_c	Distance from the detector to the chopper
x_D	Distance defined in Appendix IV
x_o	Distance from orifice exit plane to point from which streamlines appear to emanate

x_T	Distance from detector to target
β	Angle defined in Appendix IV
γ	Specific heat ratio
$\Delta\theta$	$\theta_{spec} - \theta_{r_{max}}$
δ	Angle defined in Appendix IV
θ	Angle between centerline and streamline in free-jet expansion
θ_i	Incidence angle of the molecular beam on the target
θ_r	Angle of reflection
$\theta_{r_{max}}$	Angle of maximum reflected intensity
θ_{spec}	Angle of specular reflection
λ	Molecular mean free path
ρ	Density
σ	Molecular diameter

SECTION I
INTRODUCTION

Interactions between gas molecules and a surface are of primary concern in studies of adsorption, condensation, evaporation, catalysis, diffraction, accommodation, and rarefied gas dynamics. At AEDC the particle-surface interaction studies are directed toward enhancing vacuum pumping techniques as well as increasing our knowledge of the fundamental processes of the collision of an atom or molecule with a surface.

In particle-surface interaction experiments, two factors should be considered. First, the characteristics of the molecules before and after collision are important, and second, the surface should be defined in terms of crystal orientation and species present at the gas-surface interface. Defining the characteristics of the molecules before and after collision is within the scope of present capabilities (Refs. 1 and 2). However, the problem of determining the microscopic characteristics of the surface during a basic particle-surface interaction ranges from very difficult to impossible in most instances.

In previous particle-surface interaction experiments, the investigators have used several methods of defining the surface. Smith and Saltsburg continuously deposited gold films of a predetermined orientation in an ultrahigh vacuum during their experiments (Refs. 3 and 4). Moore, Datz, and Taylor cleaned their polycrystalline platinum targets by cyclic heating (Ref. 5), and other experimentalists have used single crystals of known orientation (Refs. 1 and 6). Contamination is the major obstacle to be overcome in producing and maintaining a well-defined surface. When a well-defined surface free of contamination is exposed to a beam of molecules, the beam gas may adsorb on the target, and consequently the surface cannot be explicitly defined as to the number of adsorbed atoms present. As shown in Ref. 1, the results of presumably identical experiments performed in different laboratories often do not agree. This is probably because of undetected variations in the surface. These differences further complicate the search for a theoretical model.

Even when a reliable theoretical model is developed, it probably will not be able to predict the scattering pattern resulting from a grossly contaminated, undefined surface such as those usually encountered in engineering problems. With this in mind, it seems expedient to obtain "typical" experimental data for the regions of interest which are presently out of the range of theoretical treatment. One region of interest

would be that in which there are collisions of moderately high energy (0.30- to 0.54-ev) atoms with a "dirty"[1] metallic surface at temperatures from 36 to 285°K.

The purpose of this series of experiments was to determine how gas temperature, incidence angle, and surface temperature affect the reflection of a 285 to 2500°K argon beam from a copper surface as the temperature is varied from 36 to 300°K. In order that the experimental results may be used to predict scattering from cryosurfaces common to vacuum chambers, no attempts were made to clean the surface.

SECTION II
EXPERIMENTAL EQUIPMENT

2.1 AERODYNAMIC MOLECULAR BEAM CHAMBER

The AEDC aerodynamic molecular beam chamber (Fig. 1, Appendix I) is a stainless steel cylinder, 3 ft in diameter by 6.5 ft long, which is divided into three sections by two removable bulkheads. Vacuum conditions are produced and maintained in the cell by oil diffusion pumps, 20°K gaseous-helium-cooled cryoliners, and 77°K liquid-nitrogen-cooled cryoliners. The total pumping speed for air is in excess of 500,000 liters/sec (Table I, Appendix II).

This system is capable of producing a 4-mm-diam beam entering the test chamber with a variable beam flux up to 4.0×10^{16} molecules/sec while maintaining a background pressure of 3.0×10^{-8} torr in the test chamber. During the experimental runs the operating pressures were 4×10^{-4}, 2×10^{-7}, and 3×10^{-8} torr in the nozzle, collimating, and test sections of the chamber, respectively. A complete description of the beam system and its performance is given in Refs. 7 and 8.

2.2 HIGH TEMPERATURE AERODYNAMIC BEAM SOURCE

The basic high temperature beam source is a resistance-heated tantalum tube 4 in. long and 0.25-in. OD with a wall thickness of 0.02

---

[1]A dirty surface as used in this report refers to a surface that was cleaned by washing with Freon®, but no attempt was made to eliminate the adsorbed gases and other microscopic contaminants present on the surface. However, it was exposed to a 10^{-8} torr vacuum for several hours before the data were obtained.

in. Halfway between the ends of the tube a 0.014-in.-diam hole is drilled through the wall. The beam gas enters through both ends of the tube and is expanded through the small orifice. Electrical power is supplied by large copper electrodes attached near the tube ends. A water-cooled copper heat shield was placed around the tantalum tube to protect the cryopanels from the radiating heat load (Fig. 2).

Calibration tests performed on the high temperature source before installation in the molecular beam chamber indicate that for the resultant power input, a given temperature can be repeatedly attained. Also, the time required to reach an equilibrium temperature is of the order of only a few minutes, and the source remains at this temperature without further power adjustments.

2.3 TARGET

The target for these experiments was a hand-polished copper disk. The disk was one surface of a hollow cylinder so that gaseous helium could be circulated through it. The target temperatures, which ranged from 36 to 285°K, were measured by two Chromel®-constantan thermocouples embedded in its surface.

2.4 TARGET AND DETECTOR MOVEMENT MECHANISMS

The target and detector were rotated by chain drives, which were manually controlled using mechanical feedthroughs in the test end of the chamber. The feedthroughs were fitted with vernier scales. Alignment checks before pumpdown using a laser as a light source showed that the target and detector could be reset to the same position. The overall accuracy of a given angular value was found to be ±2 deg.

2.5 DETECTION SYSTEMS

One of the major problems in molecular beam experiments is the measurement of the reflected molecular beam flux, which can be much less than the background pressure. During these experiments, background pressure was 3.0×10^{-8} torr, which is equivalent to 10^{12} molecules/sec-cm^2 striking the detector. The molecular beam intensity reflected from the target surface, however, is also on the order of 10^{12} molecules/sec-cm^2. Therefore, it is necessary that the detection system be able to distinguish the beam signal from a background noise level of equal or less intensity. To accomplish this, a modulated beam

detection system was used. This detection system consisted of (1) a mechanical chopper, (2) a quadrupole mass spectrometer, and (3) a lock-in amplifier (Figs. 3 and 4). This detector system has the capability of recovering beam intensity signals that are three orders of magnitude less than the background gas intensity. A complete description of the detector and its performance is given in Ref. 8.

The total beam flux was measured by using a miniature ionization gage. The gage was enclosed in the standard glass envelope, but in order to increase the gage sensitivity the normal 1-in.-diam opening was reduced to 6 mm (Fig. 5).

SECTION III
ANALYSIS OF THE EXPERIMENTAL TECHNIQUES AND PROCEDURES

3.1 INTRODUCTION

The first steps in studying particle-surface interactions are to define the surface conditions if possible and to evaluate the basic parameters relating to the incident atoms. In this series of tests, an aerodynamic molecular beam was used to provide the incident atoms. Therefore, the objectives of the first experiments were to define the beam characteristics.

3.2 CHARACTERISTICS OF THE BEAM

Aerodynamic beams differ from the classical oven beams in the following areas: (1) the intensity is greater, (2) the mean energy is higher, (3) the atoms in the beam can exist as single atoms or with high-speed ratios the beam atoms may form polymers held together by van der Waals forces (Ref. 9), and (4) the velocity distribution is very narrow. For instance, at Mach number 20, the velocity distribution of an aerodynamic beam is such that 80 percent of the beam molecules have a velocity that is within 5 percent of the mean velocity (Ref. 10).

3.2.1 Total Beam Flux and Polymerization in the Beam

A detailed description of the beam components and an analysis of the free-jet expansion are given in Appendix III, and typical beam performance data are shown in Fig. 6. The data in Fig. 6 were obtained

by lowering the miniature ionization gage into the beam and obtaining the gage reading as the source pressure was varied over the desired range.

The source pressure, P_o, was varied by adjusting a needle valve in the source gas supply line. Previous calibration with an oven beam source has shown that if the ionization pressure gage reading for argon is multiplied by the calibration factor of 2.5×10^{20}, the product is the total beam flux in molecules per second.

The curves in Fig. 6 indicate the change in the total beam flux as the temperature is varied from 285 to 2500°K. The drop in the beam flux at the higher source pressures is caused by polymerization in the beam and skimmer interactions. Experimental data relating to the onset of polymerization in argon beams with high source pressures are presented in Ref. 9, and skimmer interactions are discussed in Ref. 11.

Mass spectrographic measurements taken at source pressures from 1000 to 3000 torr show that detectable amounts of polymerization begin to occur at the peak in the curve (Fig. 6) and increase rapidly with increasing source pressure. The source pressure was maintained low enough to ensure that appreciable polymerization would not occur during these experiments. Therefore, the data to be presented in this investigation are for argon atoms only.

3.2.2 Intensity Cross Section of the Beam

Another factor to consider in using aerodynamic molecular beams to study particle-surface interactions is the uniformity of the beam intensity. Measurements were made with an ionization gage to determine the intensity (molecules/sec-cm^2) at various points across the beam. Data for Fig. 7 were obtained by placing a plate with a 0.014-in.-diam hole over the ionization gage opening. Readings were then taken at positions visually measured with a transit. The beam intensity distribution was as shown in Fig. 7.

3.3 SURFACE CONDITIONS

As mentioned in Section I, the surface condition is one of the most important considerations in gas-surface interaction experiments. In pure research an uncontaminated, well-defined surface is needed for mathematical purposes. However, theoreticians cannot yet mathematically describe the gas-surface interaction to the point that all types of interactions can be successfully predicted.

Since the features of the collision of a hot gas with a clean surface cannot be reliably predicted, it is hoped that experiments under "typical" conditions will bring out the salient features of such an interaction. To typify an engineering surface, a plate of polycrystalline copper was used. Initially, the target was polished with jeweler's rouge and rinsed with Freon to remove gross contaminants. Then the target was left unattended throughout the experiments in order to simulate the surface of a typical cryoliner. Therefore, the surface was subject to contamination by background gases adsorbed on the target during the experiments. The presence and possible effects of these gases are discussed in Section IV.

3.4 EXPERIMENTAL PROCEDURE

The experimental setup, as shown in Fig. 3, was used to measure the signal from the reflected argon atoms. The target could be rotated to change the angle of incidence. To change the angle of reflection at which the signal was being measured, the detector could be moved in an arc about the target. The detector was maintained in the plane defined by the incident beam and the plane normal to the target surface. Measurements made in this plane are called "in-plane" measurements and are the only kind reported in this investigation.

To obtain the values for a spatial flux distribution curve, the beam and target temperatures were first chosen and set. Then the beam stagnation pressure was adjusted to obtain the desired beam flux, which was indicated by the miniature ionization gage. The angle of incidence was set by positioning the target. Data were taken as the detector was moved through increments of 2, 5, or 10 deg. Because of the size of the detector, data could not be taken within 20 deg of the beam.

SECTION IV
DISCUSSION OF EXPERIMENTAL RESULTS

4.1 INTRODUCTION

The data presented in Figs. 8 through 16 are representative of 100 experiments performed over a time interval of three months. Polar coordinate plots were used to give a more descriptive picture of the spatial reflection patterns, and the distance along a ray is directly proportional to the signal strength. For example, a cosine spatial distribution is a circle on these graphs. Also, it should be noted that both the incident and reflected angles are measured with respect to the

surface normal. Absolute values of the signals are omitted, since the form of the curves is of interest rather than the magnitude of the signals.

For incidence angles greater than 60 deg, the geometry of the detection system affects the data. The data were corrected for this effect as described in Appendix IV.

4.2 SCATTERING PATTERNS OF AMBIENT TEMPERATURE ARGON BEAMS SCATTERED FROM AMBIENT TEMPERATURE SURFACES

With an aerodynamic beam source temperature of 285°K, the scattering pattern for an argon beam reflected from a "dirty" copper target is shown in Fig. 8. The results (Fig. 8) agree with previous results for this chamber (Ref. 12) and with the results and predictions of other researchers (Ref. 1). The data points have been adjusted using the geometrical correction factors as described in Appendix IV. The solid curve is the corresponding cosine curve. Cosine scattering patterns have been found to be characteristic of diffuse scattering, which often occurs when surfaces are rough and contaminated (Ref. 1). The cosine scattering patterns obtained with incident beam and surface temperatures of 285°K verify the accuracy and reliability of the AEDC experimental techniques (Fig. 8).

No measurements of the energy accommodation of the beam atoms with the surface were made during this series of tests. However, the shape of the scattering pattern does provide some information about the energy accommodation in gas-surface interactions. The measure of energy accommodation is given by the accommodation coefficient which is defined

$$\text{A.C.} = \frac{E_i - E_r}{E_i - E_s}$$

where E_i is the energy of the incident gas atoms, E_r is the energy of the reflected gas atoms, and E_s is the energy the reflected atoms would have if they had come to thermal equilibrium with the surface. For an A. C. of unity (complete accommodation), the gas atoms would essentially have to randomize on the surface and then be emitted with a cosine spatial distribution. Consequently, specular reflection would imply less accommodation (i. e., A. C. < 1).

Heald and Brown (Ref. 12) have reported cosine evaporation patterns for carbon dioxide molecules that condense and then evaporate, but diffuse scattering patterns do not necessarily imply complete

accommodation, as demonstrated by Smith (Ref. 13). However, the nondiffuse scattering observed during these experiments is evidence that A. C. < 1.0.

4.3 SCATTERING PATTERNS FOR HIGH TEMPERATURE ARGON BEAMS SCATTERED FROM SURFACES AT SEVERAL TEMPERATURES

Scattering patterns were obtained for beams scattered from the copper target with surface temperatures of 285, 131, 77, and 36°K. Also, the effects of the angle of incidence and the incident gas temperature were investigated.

Figure 9 presents the effect of beam temperature for an argon beam at an incidence angle of 60 deg impinging on a 285°K copper surface. As the gas temperature increases, the patterns become further removed from diffuse, indicating that the reflected argon atoms have an effective temperature above 285°K.

The effects of varying the incident beam temperature at $\theta_i = 70$ deg and with a surface temperature of 131°K are shown in Fig. 10. However, in evaluating these data, it should be noted that the curves are comparable only as to their shape because the beam intensity varied with the incident beam temperature. Also, the three sets of data were taken on different days and could not be normalized because of the day-to-day variation of the detector sensitivity. The data in Fig. 10 do clearly indicate that, at low angles of incidence, the scattering patterns are dependent on the incident beam temperature. The more specular or lobular patterns result as the beam temperature is raised.

The next surface temperature of interest was that of a liquid-nitrogen-cooled cryopanel at 77°K. The data resulting from the interaction of the argon beam with this surface were surprising. As seen in Fig. 11, the lobular characteristics present in previous high temperature beam experiments are no longer prevalent. The beam temperature variations produce only slight effects in the scattering patterns, with 77°K surfaces, and therefore the surface must be of prime importance in determining the spatial distribution of the reflected molecules.

The effect of incidence angle (Fig. 12) on the data for the surface at room temperature was examined by using a 2500°K argon beam. All three curves differ markedly from cosine and are seen to become narrower as the incidence angle increases. The high energy beam seemed to have no effect, cleaning or otherwise, on the surface, since the scattering pattern remained constant with time.

Surface conditions were changed since the surface temperature was lowered to 131°K. The results are shown in Fig. 13. Except for a slight change at the surface normal in the curves for θ_i = 45 and 60 deg that indicates a superposition of diffuse and lobular patterns, no significant change in the overall shape of the scattering patterns occurred between room temperature and 131°K. Superposition has been used by Smith and Saltsburg (Ref. 4) for the interaction of 2250°K xenon with 600°K clean gold. It is interesting that a similar effect was observed for the collision of a rare gas with such vastly different surfaces. The copper surface in Fig. 13 is colder than the surface in Fig. 12 and probably has condensed background water vapor, which could have some effect on the scattering pattern.

The angle of incidence had little effect on the reflection patterns for a 77°K copper surface. Figure 14 shows that as the incidence angle decreases, the reflected intensity increases in the neighborhood of the surface normal. This effect caused by changes in θ_i is prevalent in the previous figures, and in Fig. 14 the result is that the reflections become more diffuse as θ_i decreases (as the surface normal is approached).

Experiments at temperatures between 131 and 77°K indicate that the transition from lobular patterns at T_s = 131°K to diffuse patterns is gradual and is, in fact, not complete at T_s = 77°K. Figure 15 shows data taken for a 2500°K argon beam incident at 60°K on a 36°K copper cryosurface. The surface was 6 deg above the temperature at which the argon beam would condense. The reflection pattern is seen to be quite diffuse. Varying the incidence angle and the beam temperature had no effect on the form of the scattering pattern of Fig. 15.

Thus, the surface temperature has been varied from room temperature to just above the condensation temperature for argon in a vacuum. There was a trend for the 2500°K beam to become more diffuse as the surface temperature decreased. A limit was seemingly reached just above the critical surface temperature for condensation (Ref. 12) as the spatial distribution pattern became quite diffuse (Fig. 16).

SECTION V
COMPARISON WITH OTHER DATA

In 1957, Hurlbut reported slightly lobular patterns for the scattering of argon beams from glass and Teflon® surfaces at 373°K (Ref. 14).

His data also revealed that the scattering patterns were a function of the angle of incidence. The lobular patterns were observed at very large angles of incidence.

In an experimental study of scattering in atom-surface collisions, Acalay (Ref. 15) measured the spatial flux distribution of a 0.6-ev argon beam scattered from a brass target at 300°K. The surface of this target was prepared (machined and polished) using standard shop techniques, and no other cleaning techniques were employed. For a 60-deg incident angle a subspecular highly lobular scattering pattern was observed. In our experiments, a supraspecular scattering pattern which was much broader than Acalay's was observed (Fig. 10) for a 2500°K (0.54-ev) argon beam impinging on a 285°K copper target at 60-deg angle of incidence.

Smith and Saltsburg (Ref. 4) have studied the scattering of rare gases from "clean" metal surfaces, e.g., from continuously deposited gold (111). For a 2500°K argon beam impinging at a 50-deg incident angle on 560°K gold (111), highly lobular, very narrow, specular scattering was observed.

The data presented in Section IV covered a range of surface temperatures from room temperature to 36°K, and the effects of incidence angle and beam temperature were discussed. Perhaps the best way to evaluate the data is to compare it with the list of general characteristics that Stickney has compiled from his survey (Ref. 1) of experimental work in gas-surface interactions. First, a few definitions and notations will be introduced.

In a lobular scattering pattern, the angle at which the maximum reflected signal occurs is measured from the surface normal and is designated $\theta_{r_{max}}$. The specular angle, θ_{spec}, is the reflection angle which equals the incidence angle, and $\theta_{spec} - \theta_{r_{max}} = \Delta\theta$. If $\Delta\theta < 0$, the lobe is supraspecular; if $\Delta\theta > 0$, the lobe is subspecular.

The eight general characteristics listed by Stickney are summarized below.

Characteristic 1 $$\frac{\partial(\Delta\theta)}{\partial T_g} \leq 0$$

Characteristic 2 $$\frac{\partial(\Delta\theta)}{\partial T_s} \geq 0$$

Characteristic 3	$\frac{\partial (\theta_{r_{max}})}{\partial \theta_i} \geq 0$
Characteristic 4	$\frac{\partial (\Delta\theta)}{\partial M_g} > 0$ when $\Delta\theta > 0$; $\frac{\partial (\Delta\theta)}{\partial M_g} < 0$ when $\Delta\theta < 0$
Characteristic 5	The dispersion of the scattering patterns increases with M_g.
Characteristic 6	Supraspecular patterns are most likely to occur when both $T_g > T_s$ and $\theta_i \ll 90$ deg.
Characteristic 7	Nondiffuse scattering patterns are most likely to result from target surfaces that are smooth and free of gross contamination.
Characteristic 8	The dispersion of nondiffuse scattering is greater for the in-plane pattern than for the out-of-plane pattern.

The first three characteristics may be derived by momentum and energy conservation and the assumption that the tangential momentum is unchanged during the interaction. Consider a "hard cube" model shown in Fig. 17 (Ref. 1). It can be reasoned that for a fixed surface temperature and angle of incidence, a positive change in gas temperature results in a negative change in $\Delta\theta$ or $\frac{\partial \Delta\theta}{\partial T_g}$. In like manner, it follows that $\frac{\partial \Delta\theta}{\partial T_s} \leq 0$ and $\frac{\partial \theta_{r_{max}}}{\partial \theta_i} \geq 0$.

In this discussion Characteristics 1, 2, 3, 6, and 7 are applicable. From Characteristic 1, if the gas temperature is increased, all other variables remaining constant, then the value of $\Delta\theta$ should decrease. Gathering information from Figs. 9, 11, and 12 and plotting the results in Fig. 18a, Characteristic 1 is shown to be present in the experimental results. It is also noticed that the peak of the lobes shifted from supraspecular to subspecular as the surface temperature decreased from 285 to 131°K. During this temperature change, water vapor, a prevalent background gas, condensed onto the surface.

Insufficient data points are available for comparison with Characteristic 2; however, as the surface temperature decreased from 285 to 131°K, a slight shift toward the surface was observed as shown by the data in Fig. 17.

Characteristic 3 is plotted in Figs. 18b and c. In this case also, the present data demonstrate the same trends as the data reviewed by Stickney. In spite of the fact that none of the lobes peaked at the specular angle, it is interesting to note that both plots have a slope of very nearly unity.

The first condition of Characteristic 6, i.e., $T_g > T_s$, was met in these experiments, but the second, $\theta_i << 90$ deg, was not. Nevertheless, supraspecular patterns did occur in some of the cases in which lobes were present. An interesting change takes place for the 2500°K beam and 131°K surface in Figs. 11 and 12. The lobes shifted from supraspecular to very slightly subspecular when the incidence angle was changed from 60 to 70 deg. The lobe position appears to be affected by incidence angle under these conditions.

Characteristic 7 is not exemplified by the majority of this data. Many nondiffuse patterns were observed, and no clean surfaces were used. In view of the fact that the first four characteristics were significantly applicable, it is somewhat encouraging that Characteristic 7 was not followed, because it seems that with the beam and surface combination used here, the unclean surface is yielding results that are normally in the domain of clean surfaces. If this were true, then the theory used for clean surfaces could be cautiously and qualitatively applied to dirty polycrystalline surfaces interacting with high temperature gases. However, the AEDC data show that as the surface became colder, the scattering patterns became more diffuse. It is conjectured that this was the result of the colder surfaces condensing more background gases and hence becoming more contaminated.

SECTION VI
SUMMARY

The AEDC argon-copper scattering experiments have shown that lobular scattering can occur during low energy gas surface interactions. Strong lobular patterns were observed for 0.30- to 0.54-ev beams of argon scattered from dirty copper surfaces at temperatures from 285 to 131°K. The scattering patterns were dependent on the incident beam

energy and the angle of incidence. Low angles of incidence and high incident beam temperature result in spatial distributions with strong lobular patterns. However, when the incident source gas temperature was less than 1400°K, the scattering patterns were cosine during all of the tests, but no data were obtained for incidence angles greater than 70 deg.

Experiments to determine the effects of the surface temperature on the scattering patterns were performed. These experiments revealed that with incidence source gas temperatures of 2500°K, the scattering patterns became more lobular as the surface temperature was decreased from 285 to 131°K. However, with a surface temperature of 77°K, the scattering pattern was only slightly lobular, and at a surface temperature of 36°K cosine scattering was observed.

These AEDC data have shown that lobular scattering patterns are more common to the physical world than had been predicted. Therefore, it now seems necessary to investigate the low energy gas-"dirty" surface collision phenomenon in detail because of the widespread engineering application to processes such as vehicle drag, heat transfer, gas adsorption, gas condensation, and cryopumping.

REFERENCES

1. Stickney, R. E. "Atomic and Molecular Scattering from Solid Surfaces." Advances in Atomic and Molecular Physics, Bates, D. R. and Esterman, I. (Ed.), Vol. 3, Academic Press, New York, 1967, pp. 143-204.

2. Saltsburg, H., Smith, J. N., Jr., and Rogers, M. (Ed.), Fundamentals of Gas-Surface Interactions. Academic Press, New York, 1967.

3. Smith, J. N., Jr. and Saltsburg, H. "Atomic-Beam Scattering from Epitaxially Grown Gold Films." Journal of Chemical Physics, Vol. 40, June 15, 1964, pp. 3585-3591.

4. Smith, J. N., Jr. and Saltsburg, H. "Recent Studies of Molecular Beam Scattering from Continuously Deposited Gold Films." Proceedings of the Fourth International Symposium on Rarefied Gas Dynamics, de Leeuw, J. H. (Ed.), Vol. 11, Academic Press, New York, 1966, pp. 491-504.

5. Moore, G. E., Datz, S., and Taylor, E. H. "Reflection and Thermal Accommodation of Helium Beams on Platinum." Journal of Catalysis, Vol. 5, April 1966, pp. 218-223.

6. O'Keefe, D. R. "The Scattering of High Energy Argon Atoms from a Well Characterized (100) Tungsten Surface." OTIAS Report No. 132, July 1968.

7. Brown, R. F. and Heald, J. H., Jr. "Description and Performance of a Molecular Beam Chamber Used for Cryopumping and Adsorption Pumping Studies." AEDC-TR-66-135 (AD641388), October 1966.

8. Heald, J. H., Jr. "Performance of a Mass Spectrometric Modulated Beam Detector for Gas-Surface Interaction Measurements." AEDC-TR-67-35 (AD648984), March 1967.

9. Brown, R. F. and Busby, M. R. "Molecular Beam Studies of Polymerization and Condensation in Free-Jet Expansions of Argon and Nitric Oxide." AEDC-TR-68-245 (AD843325), November 1968.

10. Anderson, J. B., Andres, R. P., and Fenn, J. B. "Supersonic Nozzle Beams." Advances in Chemical Physics, Ross, J. (Ed.), Vol. X, John Wiley and Sons, Inc., New York, 1966, pp. 275-318.

11. Brown, R. F. and Heald, J. H., Jr. "Background Gas Scattering and Skimmer Interaction Studies Using a Cryogenically Pumped Molecular Beam Generator." Rarefied Gas Dynamics Symposium, Brundin, C. L. (Ed.), Academic Press, New York, Vol. 2, 1967, p. 1407.

12. Heald, J. H., Jr. and Brown, R. F. "Measurements of Condensation and Evaporation of Carbon Dioxide, Nitrogen, and Argon at Cryogenic Temperatures Using a Molecular Beam." AEDC-TR-68-110 (AD674596), September 1968.

13. Smith, J. N., Jr. "Scattering of Atomic Beams by Polycrystalline Nickel." The Journal of Chemical Physics, Vol. 40, No. 9, May 1, 1964, pp. 2520-2527.

14. Hurlbut, F. C. "Studies of Molecular Scattering at the Solid Surface." Journal of Applied Physics, Vol. 28, No. 8, August 1957, p. 844-50.

15. Acalay, J. A. and Knuth, E. L. "Experimental Study of Scattering in Particle-Surface Collisions with Particle Energies of the Order of 1 ev." Proceedings of the Fifth International Symposium on Rarefied Gas Dynamics. Brundin, C. L. (Ed.), Vol. I, Academic Press, New York, 1967, pp. 253-268.

16. Ashkenas, H. and Sherman, F. S. "The Structure and Utilization of Supersonic Free Jets in Low Density Wind Tunnels." Proceedings of the Fourth International Symposium on Rarefied Gas Dynamics, de Leeuw, J. H. (Ed.), Vol. II, Academic Press, New York, 1966, pp. 84-105.

APPENDIXES

I. ILLUSTRATIONS
II. TABLES
III. FREE-JET EXPANSION
IV. DETECTOR BLOCKAGE

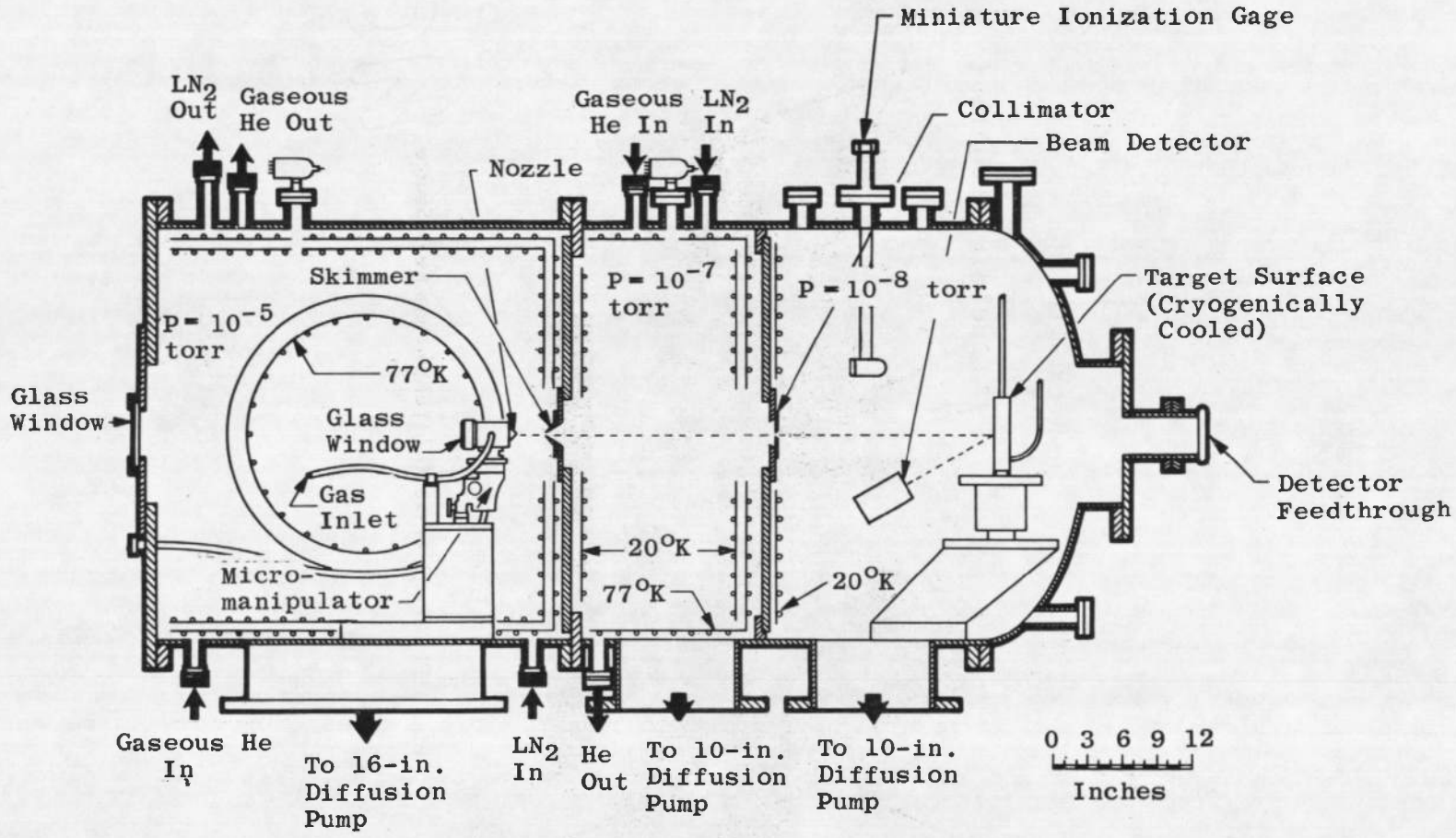

Fig. 1 Molecular Beam Chamber

AEDC-TR-69-142

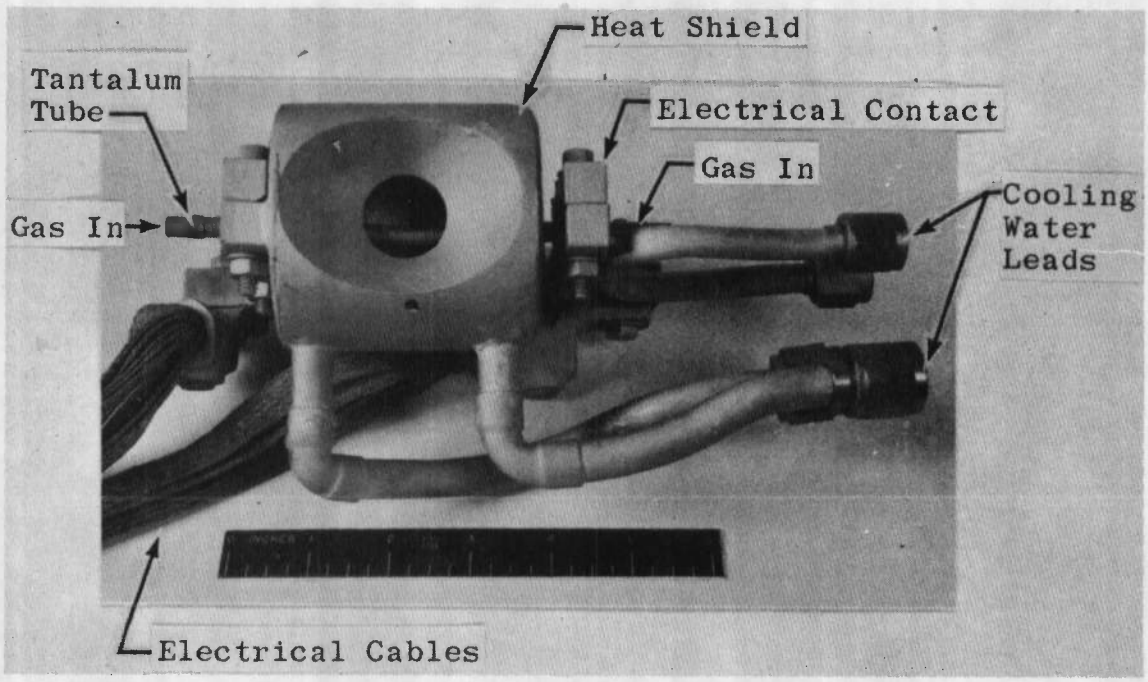

Fig. 2 Photograph of the High Temperature Beam Source

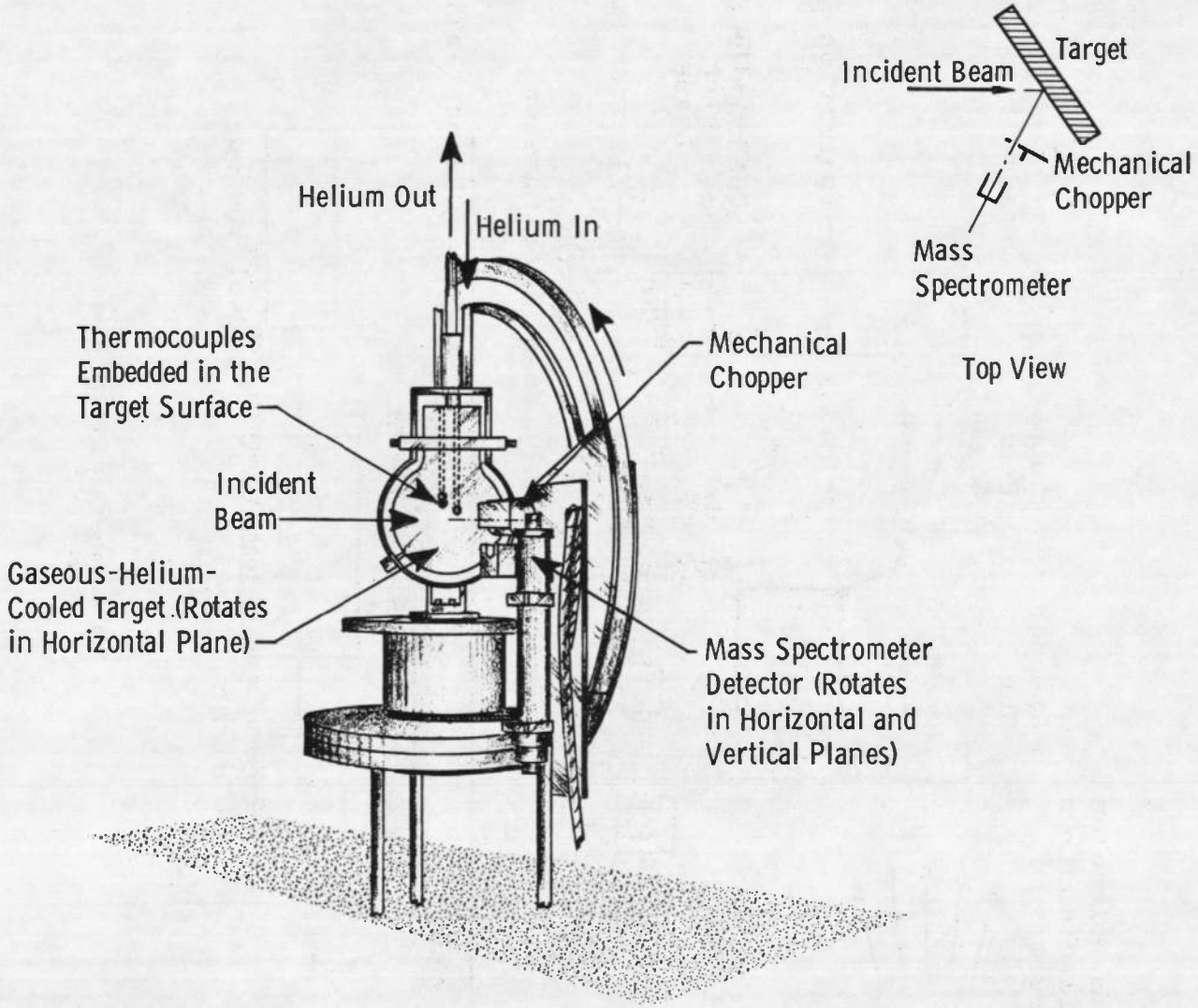

Fig. 3 Schematic of the Detector System Components

AEDC-TR-69-142

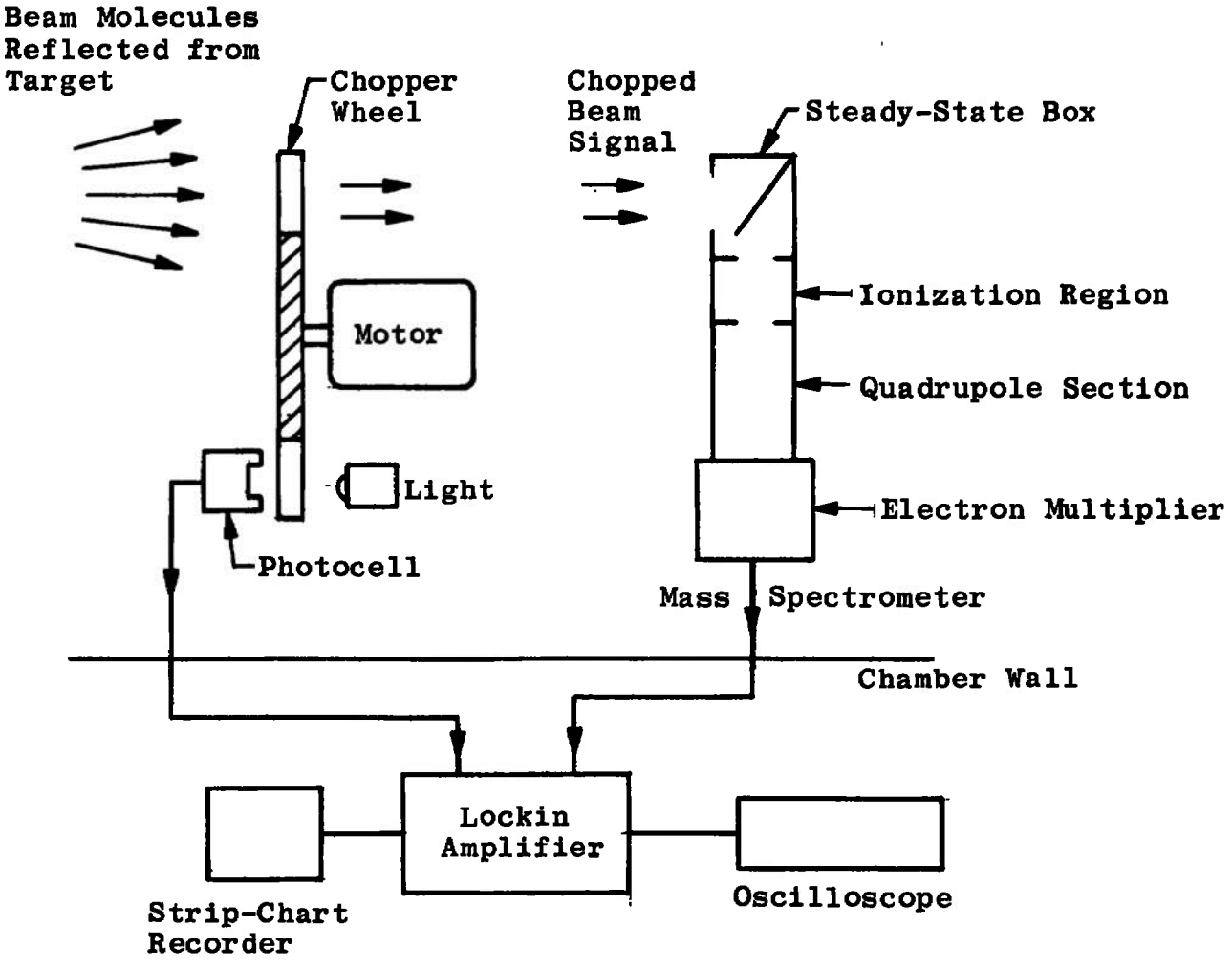

Fig. 4 Target and Detector Assembly

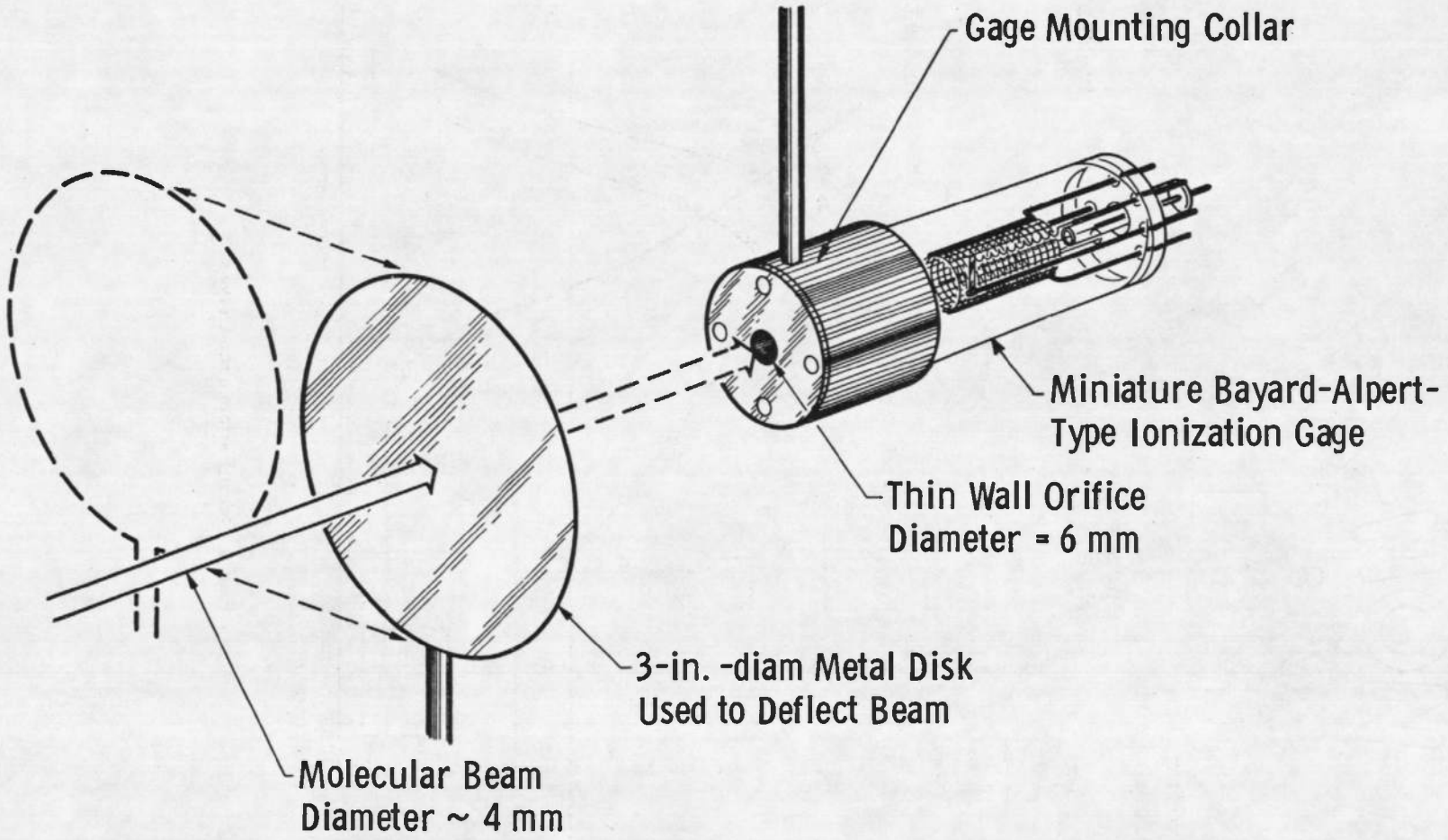

Fig. 5 Molecular Beam Detector

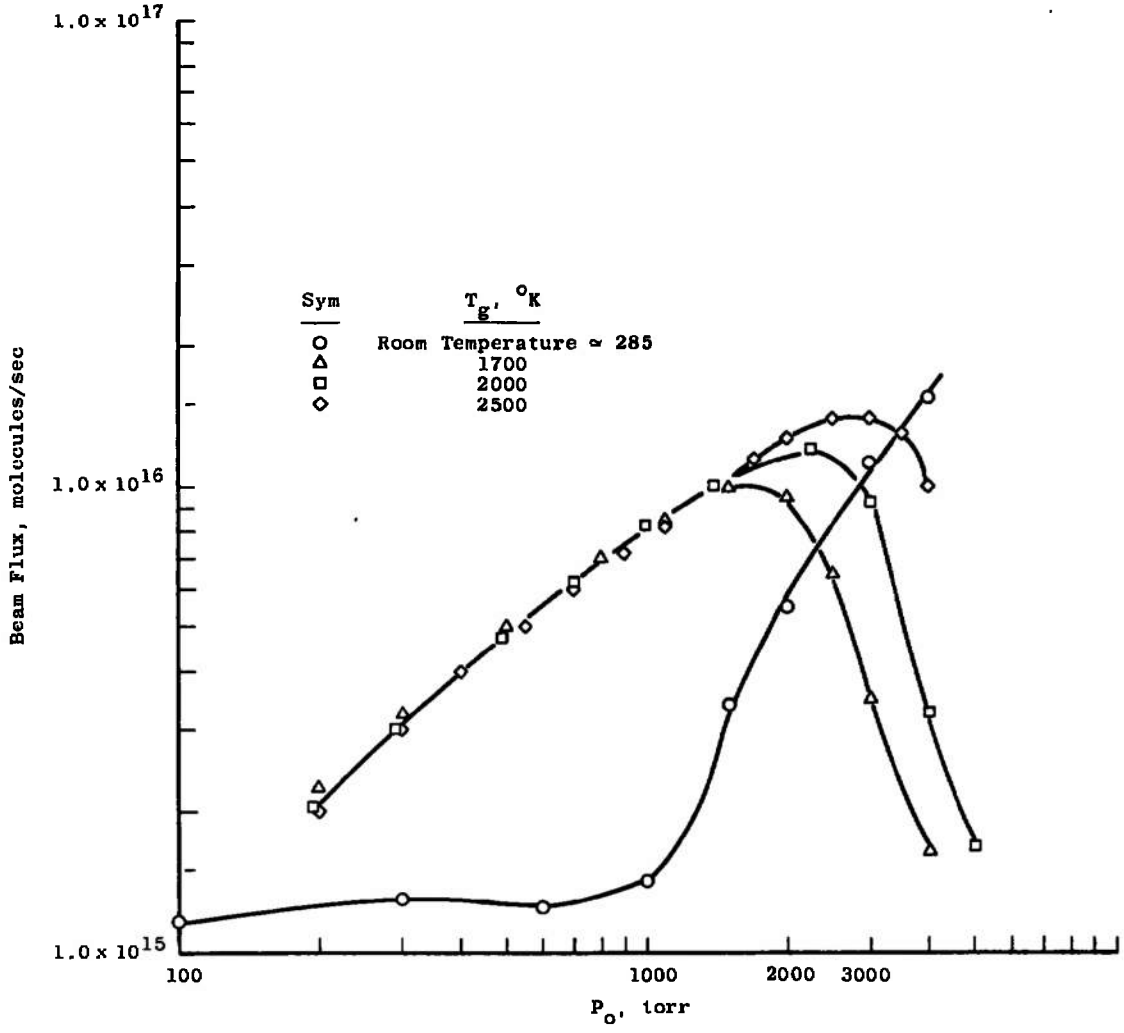

Fig. 6 Beam Performance Curves

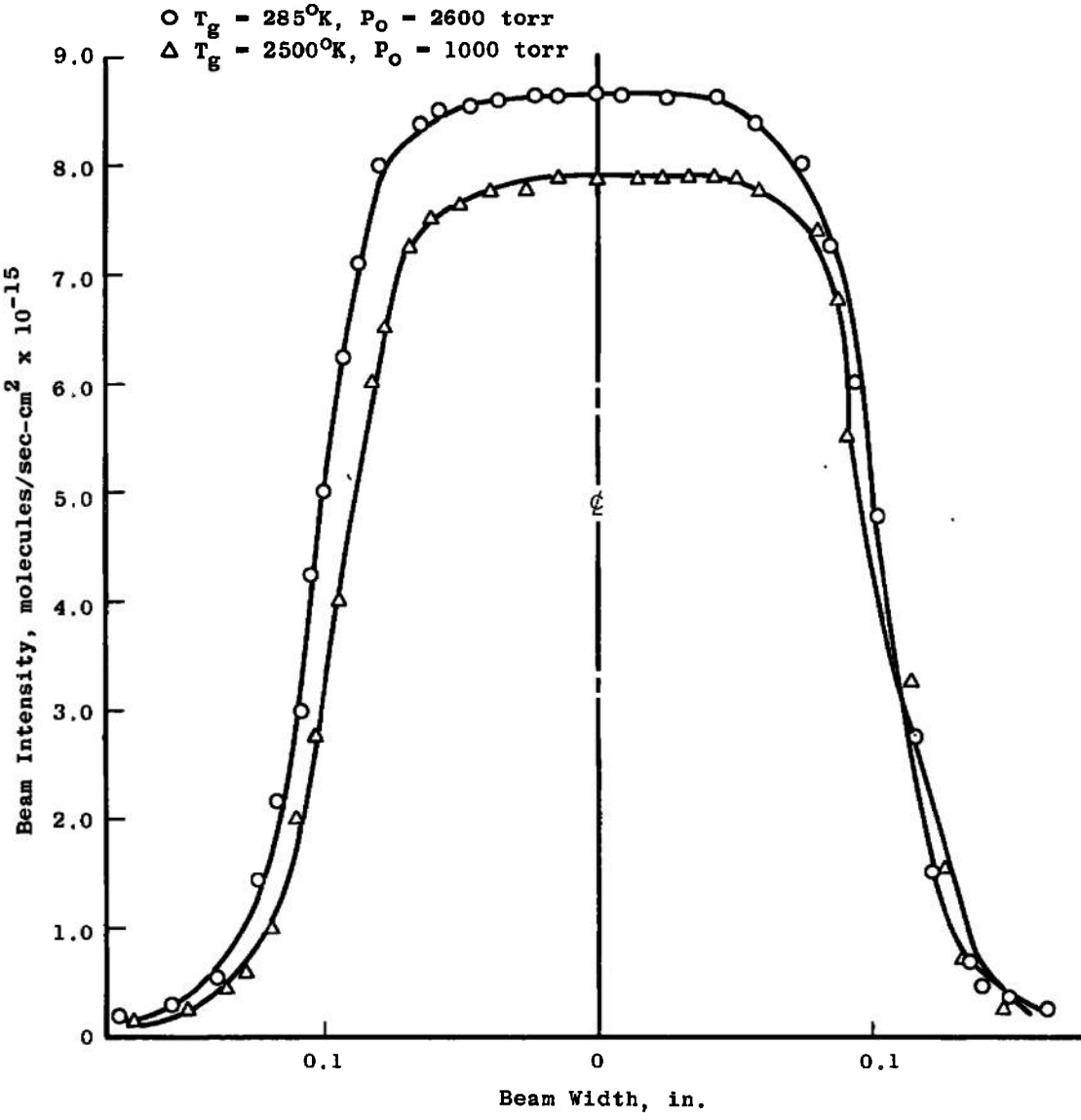

Fig. 7 Intensity Cross Section of the Beam

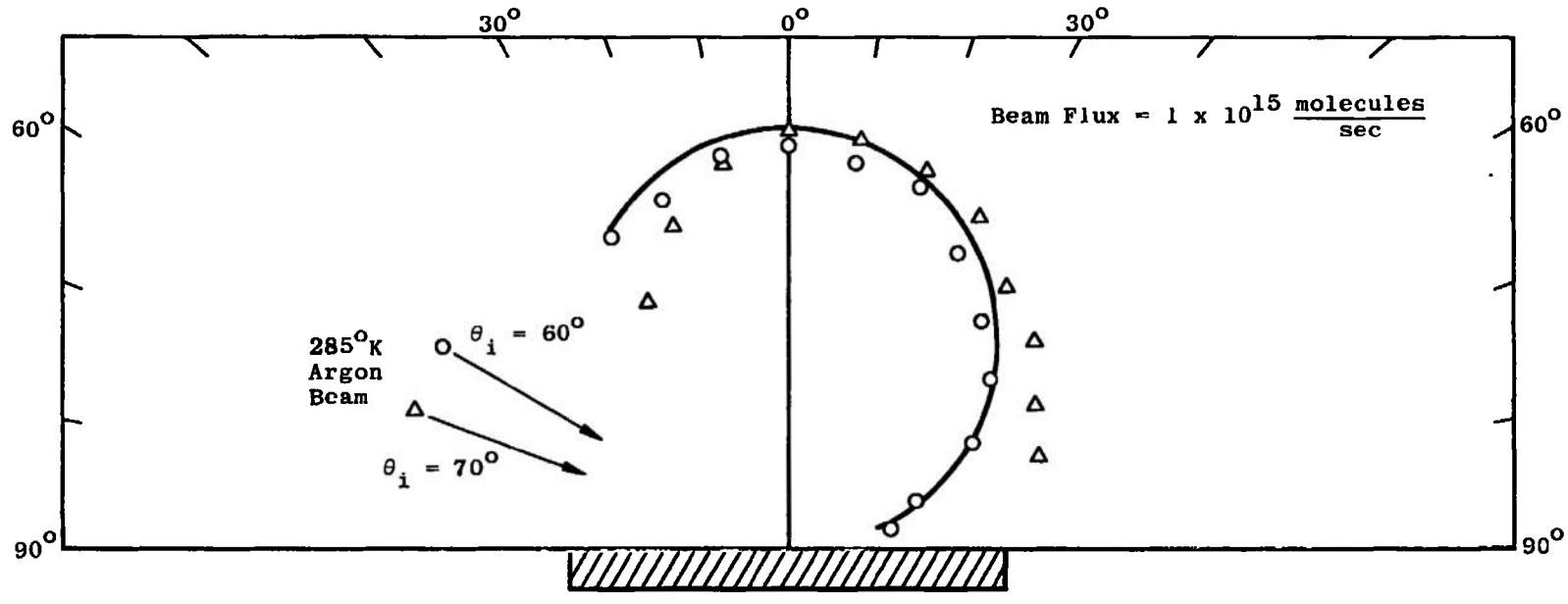

Fig. 8 Spatial Flux Distribution of 285°K Argon Reflected from 285°K Copper Surface

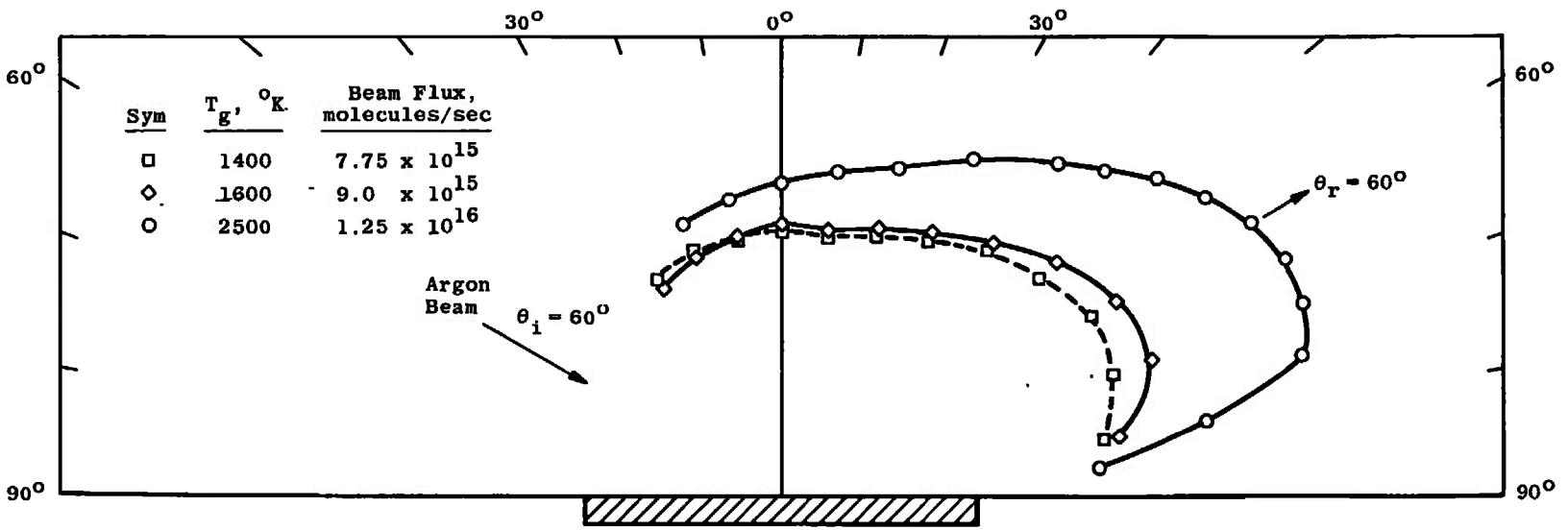

Fig. 9 Beam Temperature Effects for Argon on 285°K Copper

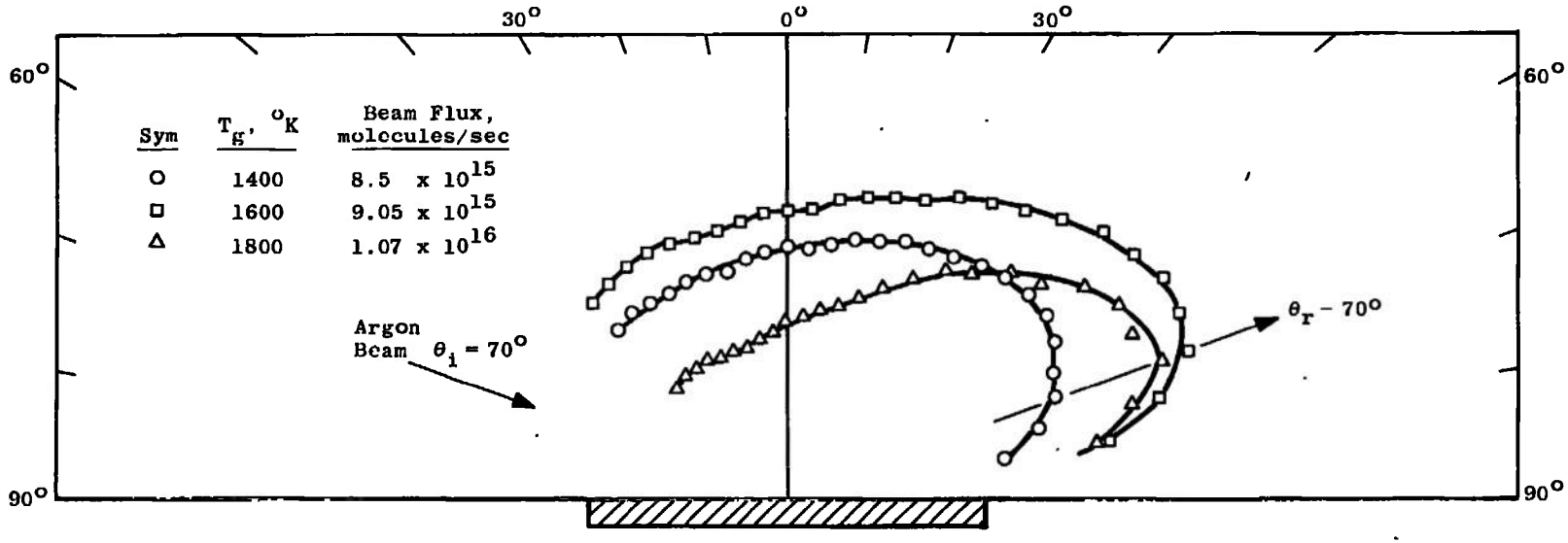

Fig. 10 Angle of Incidence Effects for 2500°K Argon on 285°K Copper

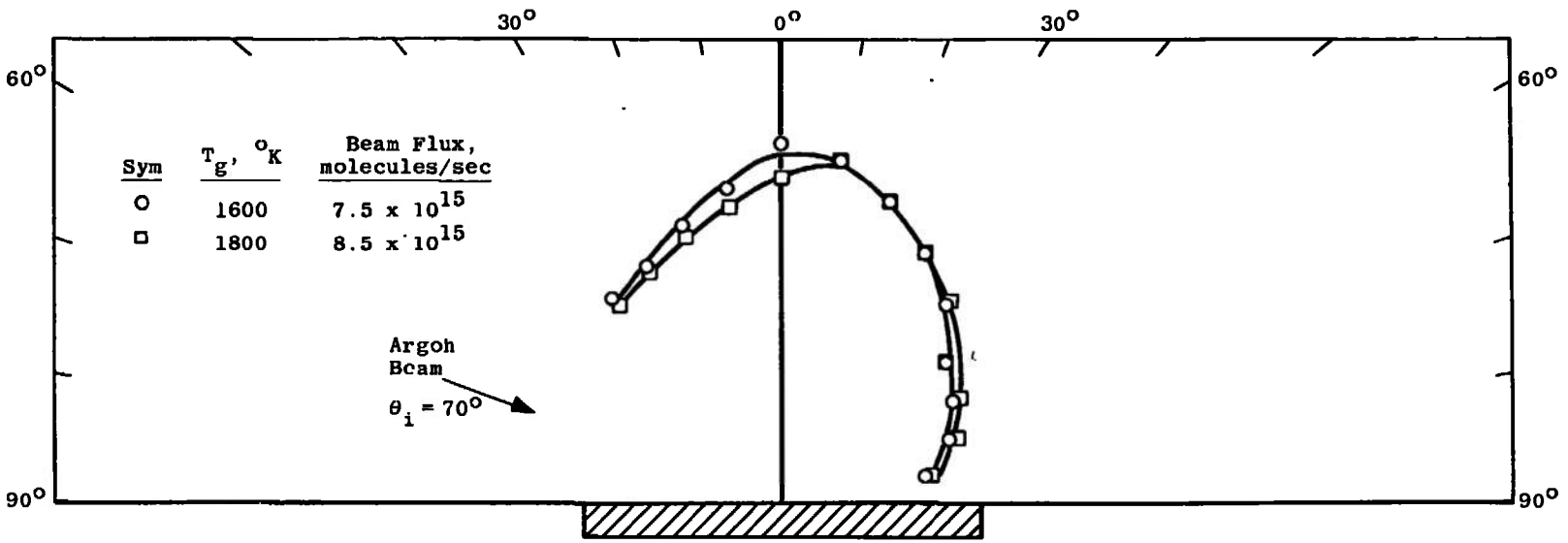

Fig. 11 Angle of Incidence Effects for 2500°K Argon on 131°K Copper

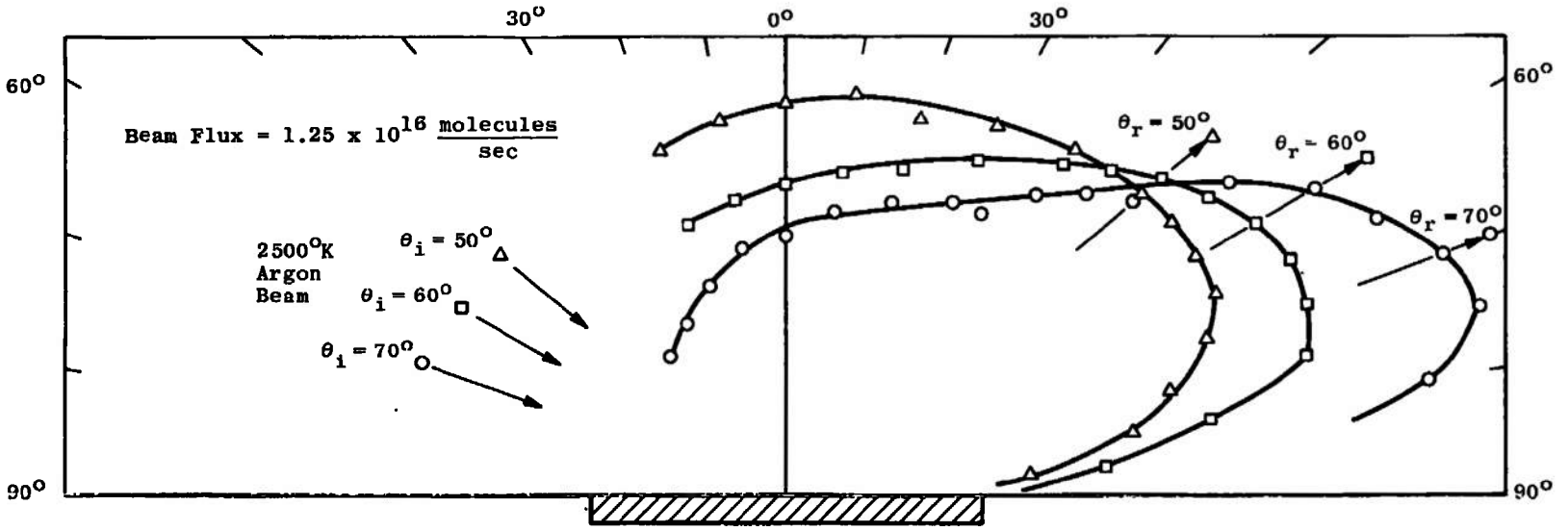

Fig. 12 Gas Temperature Effects of Argon on 131°K Copper

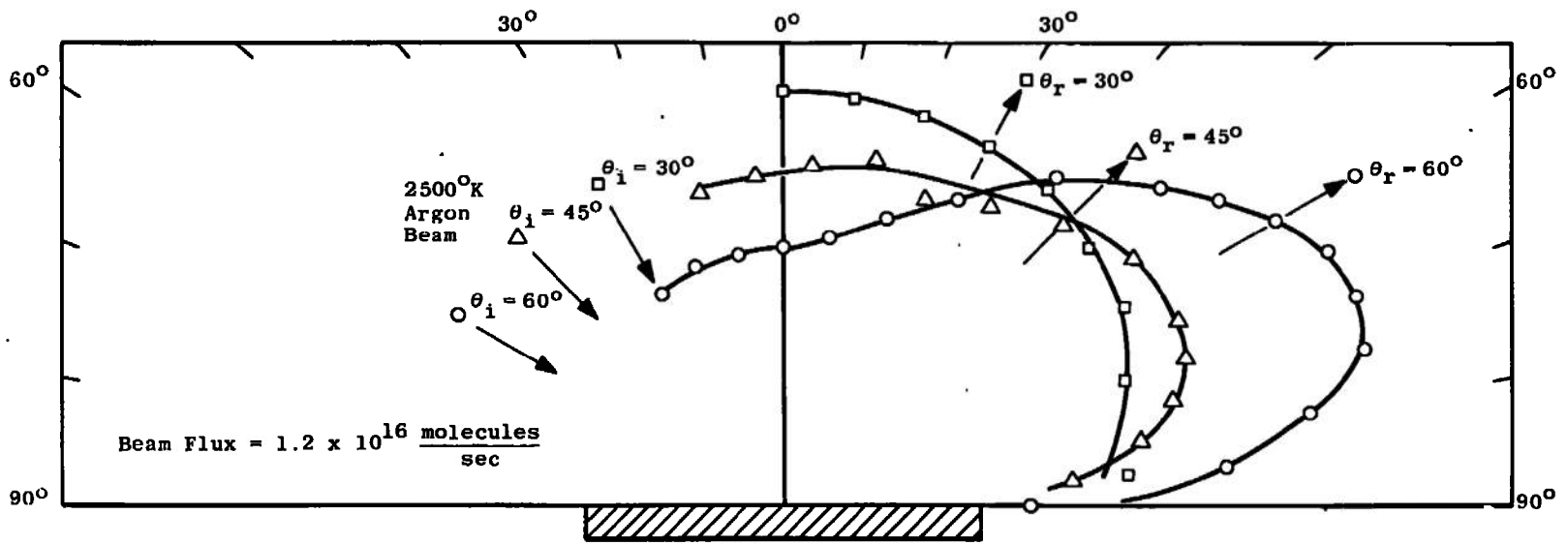

Fig. 13 Gas Temperature Effects of Argon on 77°K Copper

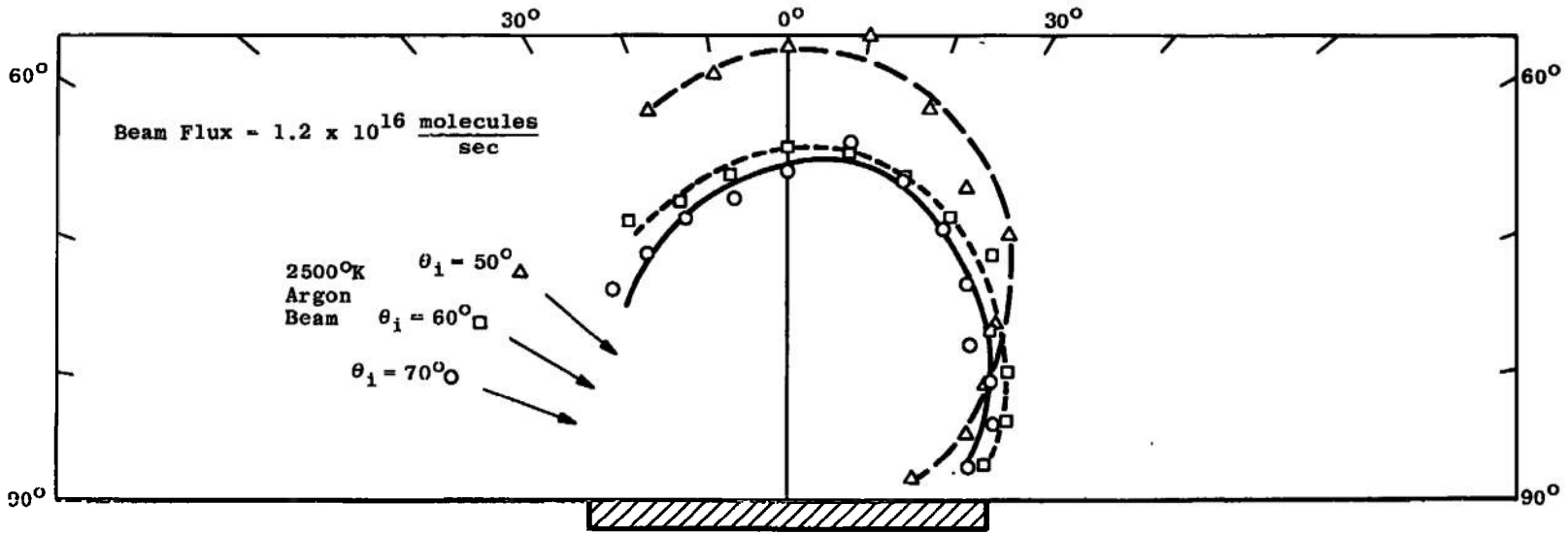

Fig. 14 Angle of Incidence Effects for 2500°K Argon on 77°K Copper

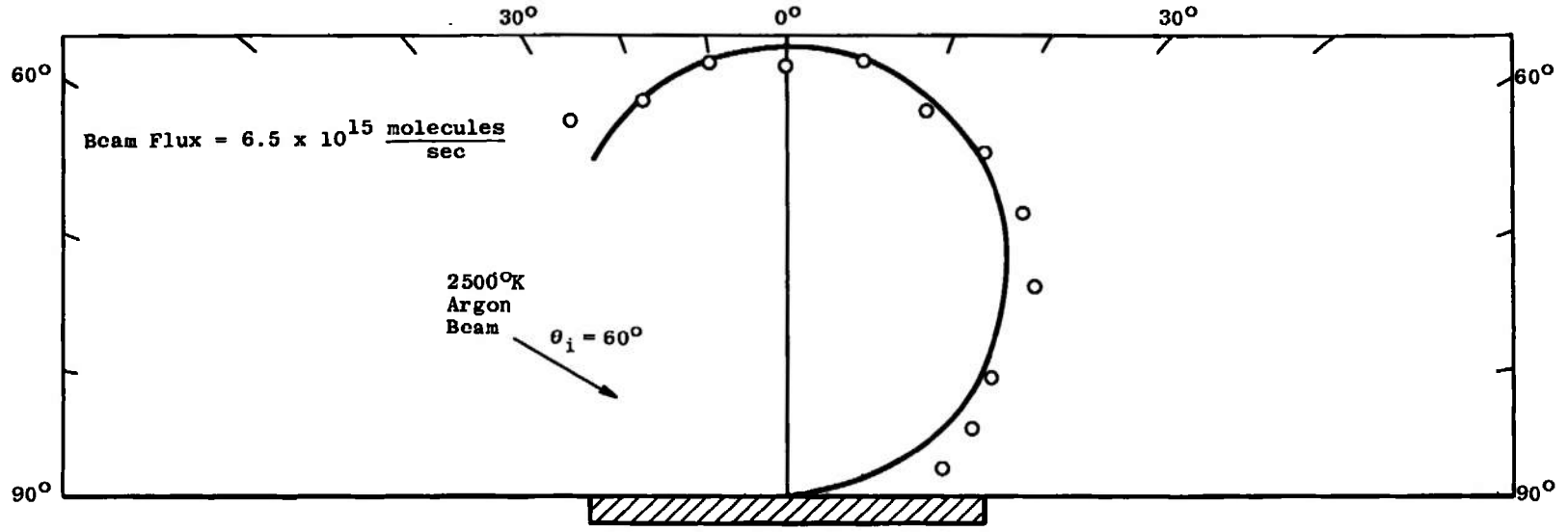

Fig. 15 Spatial Flux Distribution of 2500°K Argon Reflected from a 36°K Copper Surface

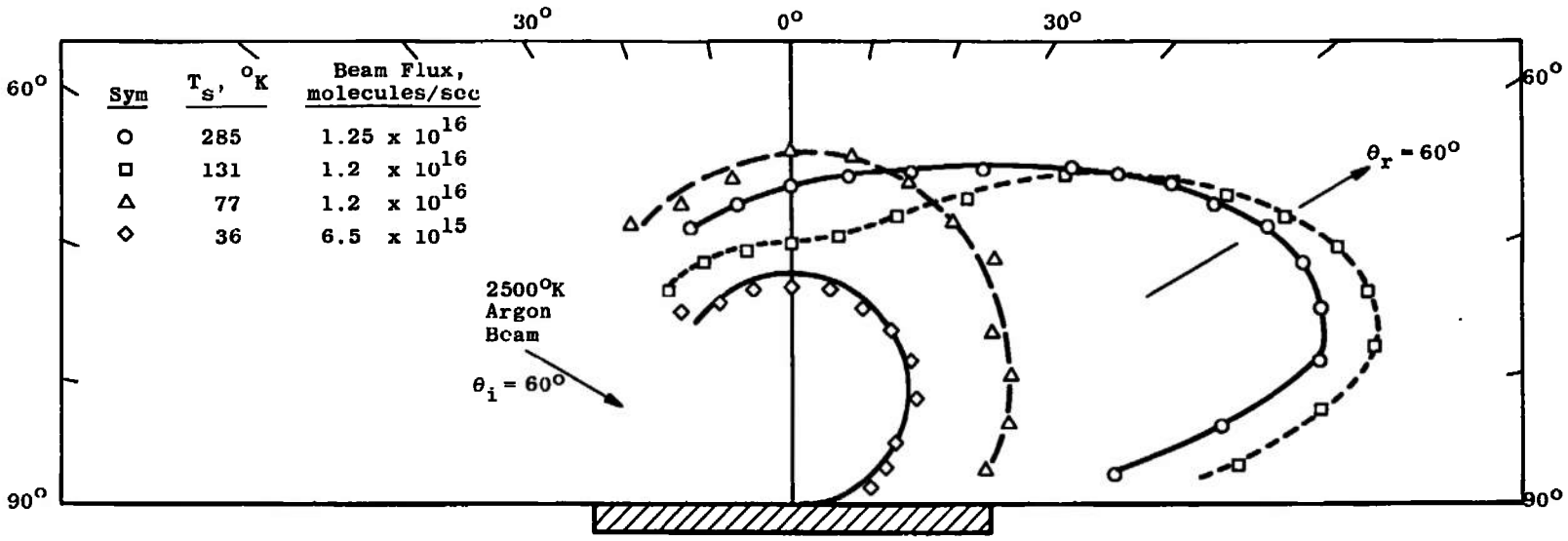

Fig. 16 Surface Temperature Effects for 2500°K Argon Reflected from Copper

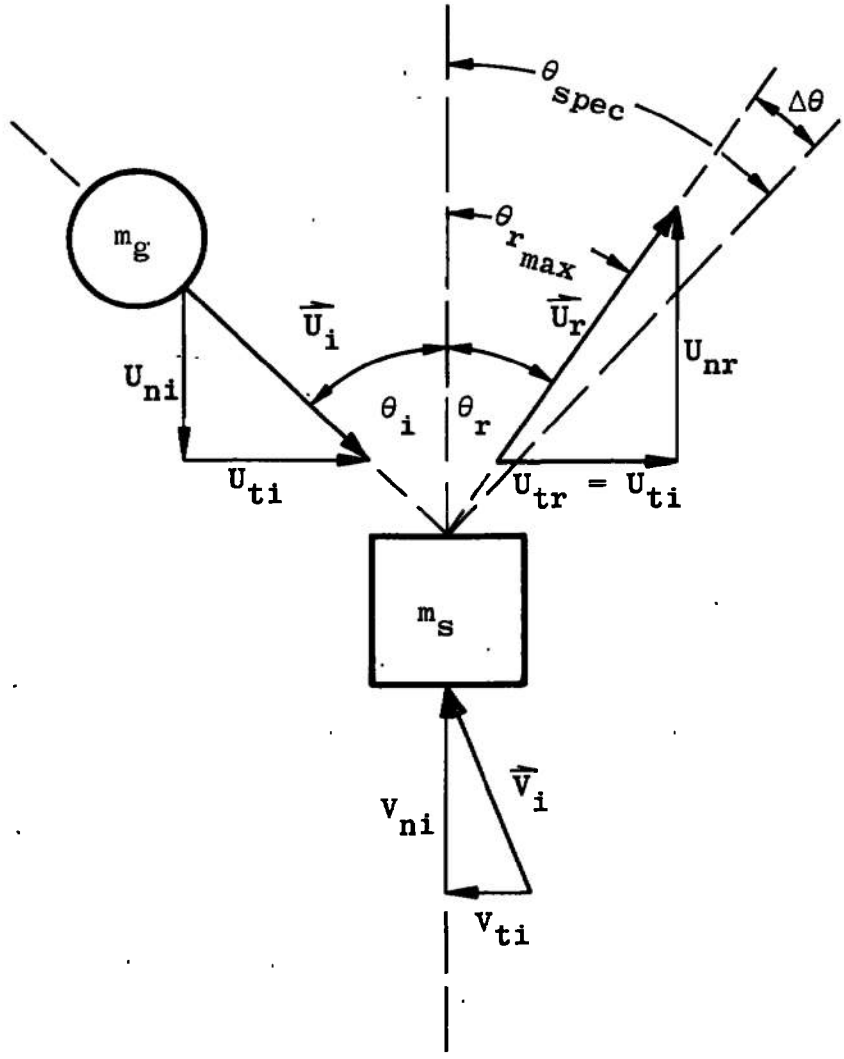

Fig. 17 Schematic Representation of the "Hard Cube" Model

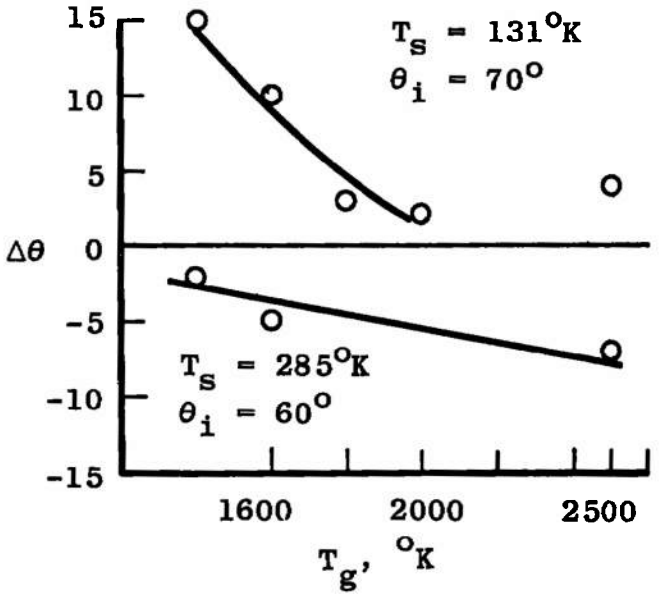

a. Characteristic 1

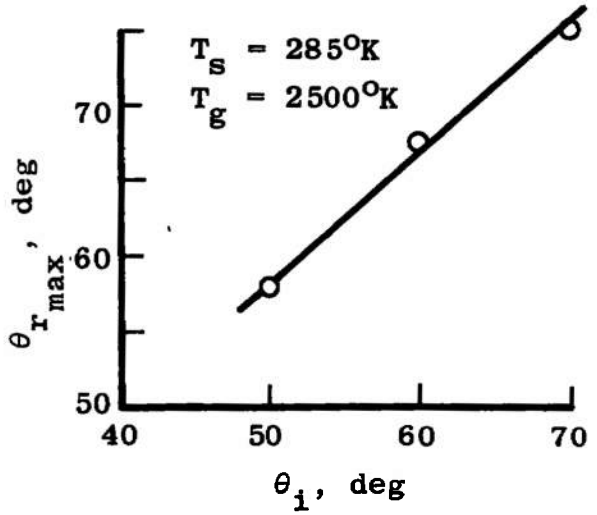

b. Characteristic 2

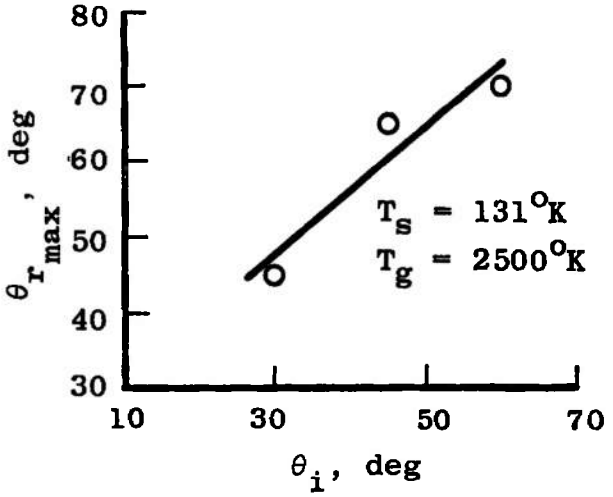

c. Characteristic 3

Fig. 18 Characteristic Trends of the Experimental Data

TABLE I
PUMPING SYSTEM DATA

Chamber Section	Pumping System	Nominal Pumping Speed, liters/sec	Operating Pressure, torr
Nozzle	16-in. Oil Diffusion Pump 20°K Gaseous -Helium Cryoliner 77°K Liquid-Nitrogen Cryoliner	2000* 270,000* 270,000**	10^{-4} to 10^{-7}
Collimation	10-in. Oil Diffusion Pump 20°K Gaseous -Helium Cryoliner 77°K Liquid-Nitrogen Cryoliner	2000* 185,000* 200,000**	10^{-7}
Test	10-in. Oil Diffusion Pump 20°K Gaseous-Helium Cryoliner 77°K Liquid-Nitrogen Cryosphere	2000* 100,000* 8000**	10^{-8}

*Pumping speed for air
**Pumping speed for carbon dioxide

TABLE II
COMPONENTS FOR GENERATING AND FORMING THE MOLECULAR BEAM

Beam Components	Description	Material	Beam Diameter, mm
Nozzle	Sonic Orifice in the Wall of a Resistance-Heated Tantalum Tube	Tantalum	0.35
Skimmer	Hallow Cone with Truncated Tip. Semivertex Angles of 30 deg Internal and 40 deg External	Stainless steel	4
Collimator	Thin Wall Orifice	Aluminum	4

APPENDIX III
FREE-JET EXPANSION

The beam geometry is shown in Table II and Fig. III-1. Alignment of the nozzle, skimmer, collimator, target, and detector system was accomplished by using a low power laser. Then, the optimum nozzle skimmer separation distance was calculated using the method given by Ashkenas and Sherman (Ref. 16) to analyze the flow field. They give the properties of a free jet at any location in the free-jet expansion. Of particular interest is the centerline Mach number which is given by:

$$M = A\left(\frac{x - x_0}{D}\right)^{\gamma-1} - \frac{1}{2}\left(\frac{\gamma+1}{\gamma-1}\right)/A\left(\frac{x - x_0}{D}\right)^{\gamma-1} \qquad \text{(III-1)}$$

where D is the orifice diameter. The constant A and the distance, x_0, from the exit plane, at which the streamlines appear to originate depend on γ. At some distance from the source the expansion goes through a transition from continuum to free molecular flow, as indicated by the Knudsen number $\frac{\lambda}{D}$ where λ is the molecular mean free path and D is a characteristic dimension. To calculate the Knudsen number, the skimmer diameter is used as the characteristic length. Then conditions can be found that will ensure free molecular flow at the skimmer entrance. This is a desirable state because interactions between the beam gas molecules and the skimmer surfaces will be minimized.

To calculate the distance at which the Knudsen number becomes greater than ten, we will use

$$\lambda = \frac{1}{\sqrt{2\pi\sigma^2 n}}$$

which is based on a Maxwellian velocity distribution. In the denominator, σ is the molecular diameter and n is the number density, which can be expressed

$$n = \rho/m$$

So now we have

$$\lambda = \frac{m}{\sqrt{2\pi\sigma^2\rho}} \qquad \text{(III-2)}$$

Equation (III-2) can be solved for ρ, and the result can be multiplied into the equation of state to give

$$\frac{\rho}{\rho_o} = \frac{m}{\sqrt{2\pi\sigma^2\lambda}} \frac{RT_o}{P_o} \qquad \text{(III-3)}$$

where the subscript o refers to stagnation conditions.

Considering the flow to be isentropic, the nozzle flow equation

$$\frac{\rho}{\rho_o} = \left(1 + \frac{\gamma - 1}{2} M^2\right)^{\frac{1}{\gamma - 1}}$$

can be solved for M, in terms of ρ_o/ρ, and this value of M can be replaced into Eq. (III-1) to solve for density ratios down the centerline. Ashkenas and Sherman give the values of A and $\frac{x_o}{D}$ as 3.26 and 0.075, respectively, for $\gamma = 1.67$, which is the accepted value for argon. The results compose a picture of the flow field as shown in Fig. III-2.

In Eq. (III-3), $R = 2.08 \times 10^6 \frac{\text{dyne-cm}}{\text{gm-°K}}$, $m = 6.65 \times 10^{-23}$ gm, and $\gamma = 1.67$, all for argon. The atomic diameter, σ, however, can be determined by two different methods. Using viscosity measurements, σ^2 is 13.3×10^{-16} cm^2, whereas determination by van der Waal's coefficient gives σ^2 as 8.67×10^{-16} cm^2.

Referring the values of $\frac{\rho}{\rho_o}$ from Eq. (III-3) to Fig. III-2, the distance downstream, in orifice diameters, at which Kn becomes greater than 10 can be found.

Knowing that the experiments would be run with source temperatures approaching 2500°K and source pressures in the range of 200 torr, it was indicated by Fig (III-2) that the skimmer should be placed 140 nozzle diameters from the nozzle for Kn_s of 10 and 50 diameters for a Kn_s of 1. Experiments with the nozzle-skimmer separation distance varying from 200 to 100 nozzle diameters revealed that the maximum beam intensity was obtained with a separation distance near 100 diameters. Therefore, the separation distance was fixed at 100 diameters. The analysis of the expected flow field is shown in Fig. III-2. As seen in Fig. III-2, slightly more than 80 percent of the gas should leave the source without collisions with the heat shield (Fig. 2).

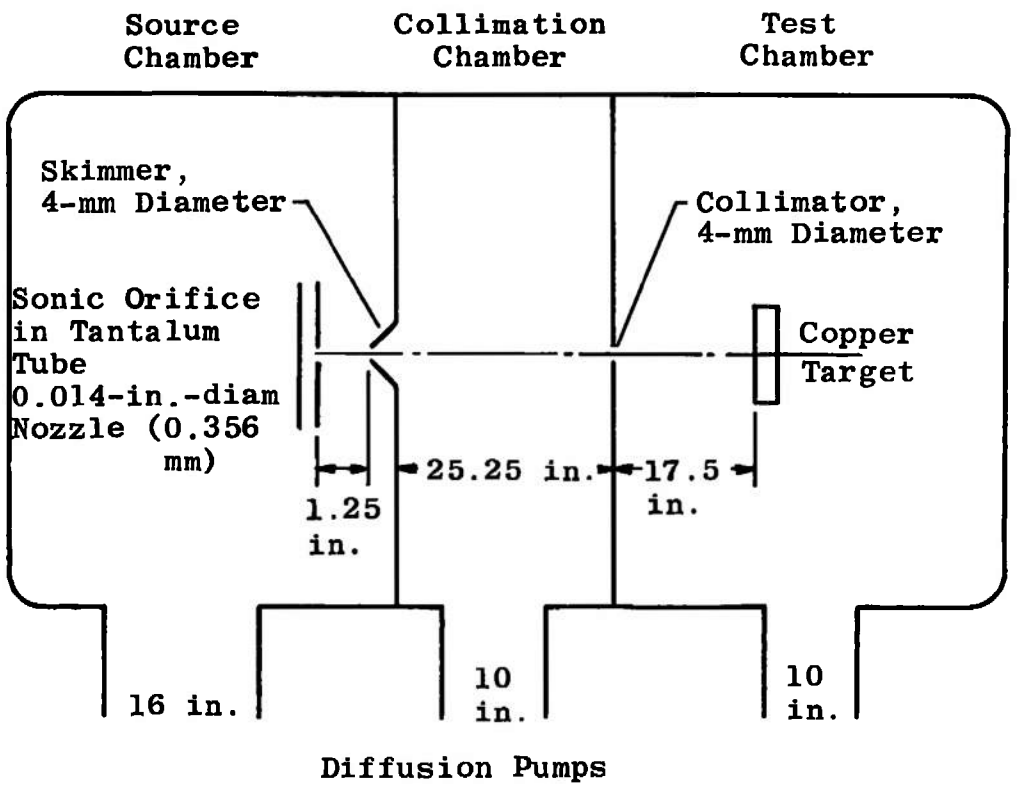

Fig. III-1 Schematic Diagram of the Chamber with Essential Dimensions

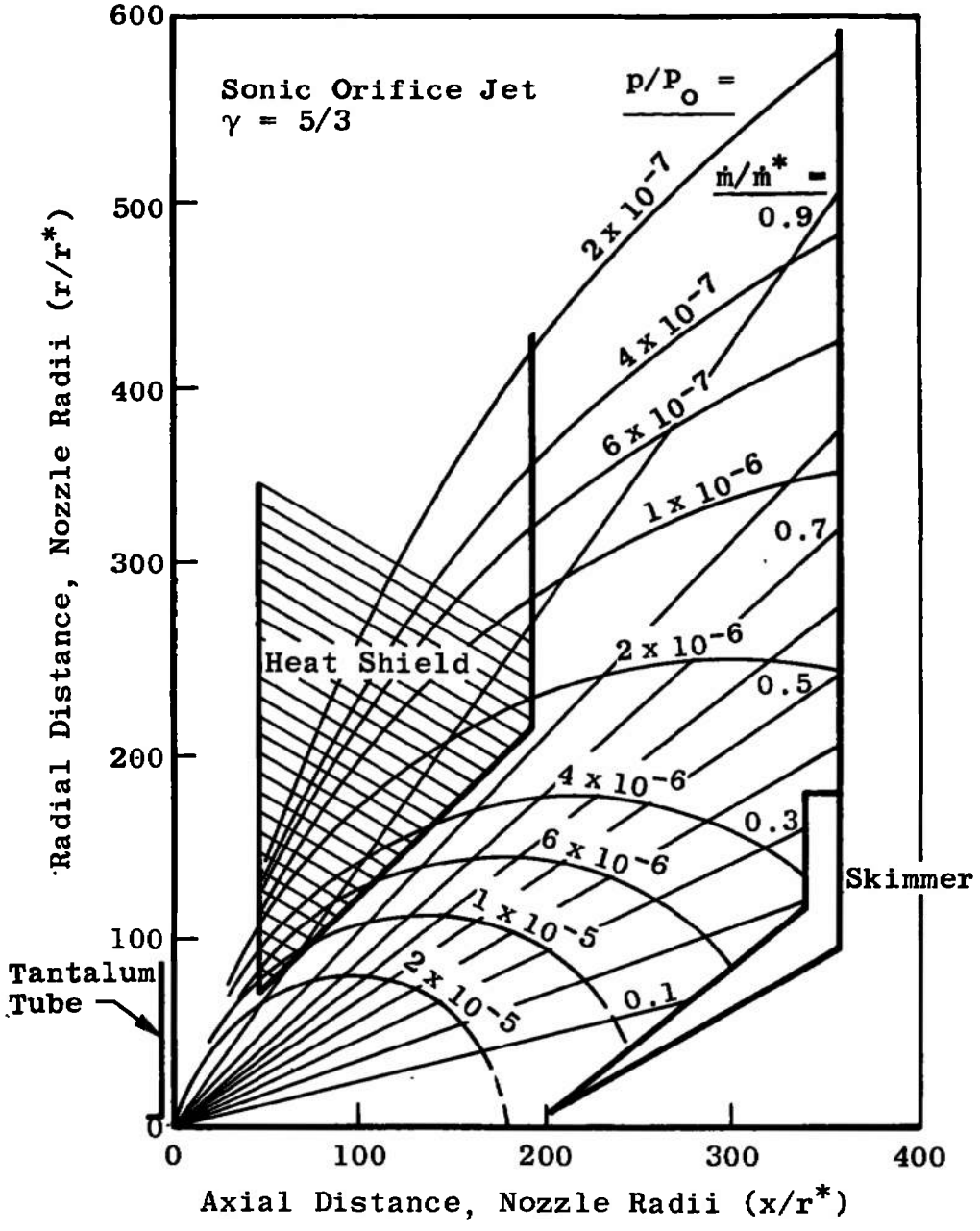

Fig. III-2 Free-Jet Expansion from a Sonic Orifice Jet

APPENDIX IV
DETECTOR BLOCKAGE

Because of the relative positions of the target, chopper wheel, and detector, the detector cannot always "see" all of the surface area that the beam strikes. Therefore, a geometric correction factor must be applied to the spatial distribution data so that for each of its positions the detector is, in effect, receiving information from the same surface area.

The geometry for the correction is shown in Fig. IV-1. The correction factor, F, will be the width of the beam spot viewed by the detector at $\theta_r \neq 0$ divided by the width of the beam spot with the beam at θ_i angle of incidence:

$$F = \frac{W_a}{W_i} \tag{IV-1}$$

To find an expression for W_a, first x_D is found by geometry:

$$\frac{W_D}{W_c} = \frac{x_D}{x_c + x_D}$$

$$x_D = \frac{W_c x_c}{W_c - W_D} \tag{IV-2}$$

Next, W_n is found

$$\frac{W_n}{W_D} = \frac{x_T + x_D}{x_D}$$

$$W_n = \frac{x_T + x_D}{x_D} W_D \tag{IV-3}$$

And by the sine law

$$\frac{1/2\ W_n}{\sin \delta} = \frac{1/2\ W_a}{\sin \omega} \tag{IV-4}$$

where

$$\delta = 180 \text{ deg} - \omega - \theta_r$$
$$\omega = 180 \text{ deg} - \beta \tag{IV-5}$$

and

$$\beta = \tan^{-1}\left(\frac{x_c + x_D}{1/2\ W_c}\right)$$

Combining Eqs. (IV-1) through (IV-5) with $\frac{W_o}{W_i} = \cos \theta_i$ gives

$$F = \frac{\sin\left[180 \text{ deg} - \tan^{-1}\left(\frac{x_c + x_D}{1/2\ W_c}\right)\right]}{\sin\left[180 \text{ deg} - \tan^{-1}\left(\frac{x_c + x_D}{1/2\ W_c}\right) - \theta_r\right]}\left[\left(\frac{x_T - x_D}{x_D}\right) W_D\right]\frac{\cos \theta_i}{W_o} \qquad \text{(IV-6)}$$

F is now expressed as a function of θ_i and θ_r at each data point. Using $W_o = 0.64$ cm, $W_c = 1.27$ cm, $W_D = 0.635$ cm, $X_c = 5.13$ cm, and $X_T = 14.19$ cm, the following table of values for F can be calculated.

θ_i = 70 deg	
θ_r	F
0	0.806
5	0.807
10	0.815
15	0.825
20	0.845
25	0.873
30	0.910
35	0.956
40	1.000

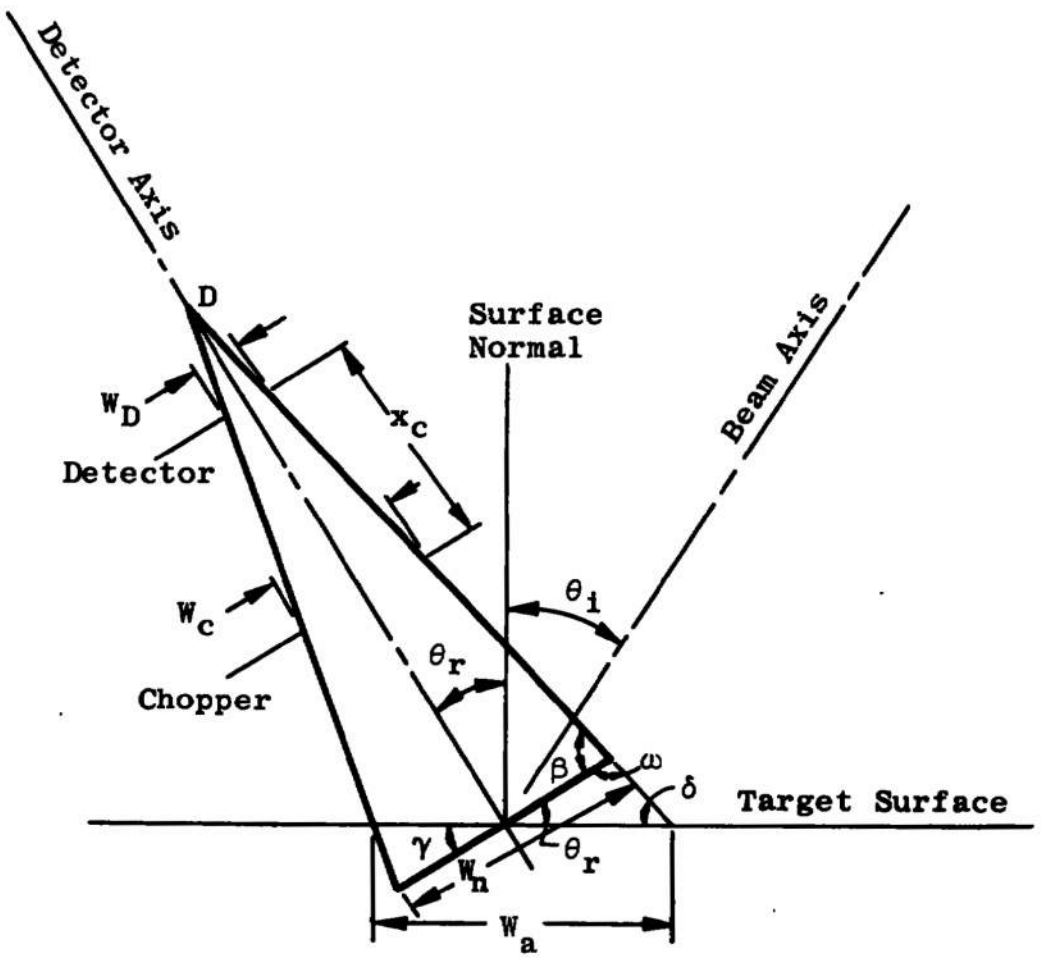

Fig. IV-1 Geometry for Calculating the Detector Correction Factor

UNCLASSIFIED

Security Classification

DOCUMENT CONTROL DATA - R & D

(Security classification of title, body of abstract and indexing annotation must be entered when the overall report is classified)

1. ORIGINATING ACTIVITY (Corporate author)	2a. REPORT SECURITY CLASSIFICATION
Arnold Engineering Development Center ARO, Inc., Operating Contractor Arnold Air Force Station, Tennessee 37389	UNCLASSIFIED
	2b. GROUP N/A

3. REPORT TITLE

SPATIAL DISTRIBUTIONS FROM 285 TO 2500°K ARGON BEAMS SCATTERED FROM AN UNDEFINED COPPER SURFACE AT TEMPERATURES BETWEEN 36 AND 285°K

4. DESCRIPTIVE NOTES (Type of report and inclusive dates)

September to November, 1968 - Final Report

5. AUTHOR(S) (First name, middle initial, last name)

R. L. Caldwell, M. R. Busby, and R. F. Brown, ARO, Inc.

6. REPORT DATE	7a. TOTAL NO. OF PAGES	7b. NO. OF REFS
December 1969	52	16

8a. CONTRACT OR GRANT NO.	9a. ORIGINATOR'S REPORT NUMBER(S)
F40600-69-C-0001	AEDC-TR-69-142
b. PROJECT NO. 8951	
c. Program Element 61102F	9b. OTHER REPORT NO(S) (Any other numbers that may be assigned this report) N/A
d.	

10. DISTRIBUTION STATEMENT

This document has been approved for public release and sale; its distribution is unlimited.

11. SUPPLEMENTARY NOTES	12. SPONSORING MILITARY ACTIVITY
Available in DDC.	Arnold Engineering Development Center, Air Force Systems Command, Arnold AF Station, Tennessee 37389

13. ABSTRACT

An aerodynamic molecular beam and a phase-sensitive detection system were used to investigate the effects of the gas temperature, incidence angle, and surface temperature on the spatial distribution from 285 to 2500°K argon beams reflected from an undefined copper surface. With an incident beam temperature less than 1400°K, cosine scattering was observed during all of the tests. However, data were not obtained for incident angles, measured with respect to the surface normal, greater than 70 deg. With incident beam source temperatures greater than 1400°K, the scattering patterns were observed to be dependent on the angle of incidence and the incident beam energy. Low angles of incidence and high beam energies (i.e., greater than 0.30 ev) result in spatial distributions with strong lobular patterns. To determine the effects of the surface temperature on the spatial distribution, several experiments were run with a 0.54-ev incident beam at surface temperature of 285, 131, 77, and 36°K. With a surface temperature of 285°K and an incidence angle of 70 deg, lobular reflection patterns were observed, and at 131°K the reflection patterns became more lobular. Then, with a surface temperature of 77°K, slightly lobular patterns were observed, and at 36°K the spatial distribution of the reflected beam was cosine. These data are the first known observations of lobular scattering patterns for low energy (i.e., 0.30- to 0.54-ev) beams scattered from contaminated surfaces at low temperatures.

DD FORM 1 NOV 68 1473

UNCLASSIFIED

Security Classification

14. KEY WORDS	LINK A		LINK B		LINK C	
	ROLE	WT	ROLE	WT	ROLE	WT
spatial distribution						
particle density (concentration)						
molecules						
vacuum pumps						
surfaces						
copper						
rare gases						
argon						
beams (radiation)						